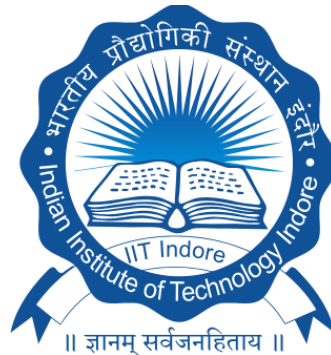


Design Optimization of Synthetic Jet Parameters for Effective Heat Transfer

MS (Research) Thesis

By

**Rahul Suryawanshi
(Roll No.: 2004103007)**



**DEPARTMENT OF MECHANICAL ENGINEERING
INDIAN INSTITUTE OF TECHNOLOGY INDORE**

July 2022

Design Optimization of Synthetic Jet Parameters for Effective Heat Transfer

A THESIS

*Submitted in fulfillment of the
requirements for the award of the degree
of*

Master of Science (Research)

by

**Rahul Suryawanshi
(Roll No.: 2004103007)**



**DEPARTMENT OF MECHANICAL ENGINEERING
INDIAN INSTITUTE OF TECHNOLOGY INDORE**

July 2022



INDIAN INSTITUTE OF TECHNOLOGY INDORE

CANDIDATE'S DECLARATION

I hereby certify that the work which is being presented in the thesis entitled **Design Optimization of Synthetic Jet Parameters for Effective Heat Transfer** in fulfillment of the requirements for the award of the degree of **Master of Science (Research)** and submitted to the **Department of Mechanical Engineering, Indian Institute of Technology (IIT) Indore**, is an authentic record of my own work carried out during the time period from August 2020 to May 2022 under the supervision of **Dr. Harekrishna Yadav** and **Dr. Satyanarayan Patel**, Assistant Professors, Department of Mechanical Engineering, IIT Indore.

The matter presented in this thesis has not been submitted by me for the award of any other degree of this or any other institute.

29/07/2022

Signature of the student with date
(RAHUL SURYAWANSHI)

This is to certify that the above statement made by the candidate is correct to the best of our knowledge.

29/07/2022

Signature of the Supervisor of
MS (Research) thesis #1 (with date)
(Dr. Harekrishna Yadav)

29/07/2022

Signature of the Supervisor of
MS (Research) thesis #2 (with date)
(Dr. Satyanarayan Patel)

RAHUL SURYAWANSHI has successfully given his MS (Research) Oral Examination, held on **29th July 2022**.

29th July 2022

Signature of Chairperson (OEB) with date

29/07/2022

29/07/2022

Signature(s) of Thesis Supervisor(s) with date

01/08/2022

Signature of Convener, DPGC with date

01/08/2022

Signature of Head of Discipline with date

ACKNOWLEDGEMENTS

I want to express my sincere gratitude to my supervisor, **Dr. Harekrishna Yadav** and co-supervisor **Dr. Satyanarayan Patel**, Assistant Professors, Department of Mechanical Engineering, Indian Institute of Technology (IIT) Indore, for the patient guidance, support, encouragement, and advice they have provided throughout my research work. I have been fortunate to have supervisors who cared so much about my work and promptly responded to my questions and queries. At many stages during this research project, I benefited from their advice, particularly so when exploring new ideas. Their careful editing contributed enormously to the production of this thesis.

I wish to express gratitude to PG progress committee members Dr. Satosh K. Sahu, Professor (HOD), Department of Mechanical Engineering, IIT Indore and Dr. Vivek Kanhangad, Associate Professor, Department of Electrical Engineering IIT Indore, for their valuable suggestions and comments during this work. I am also thankful to the Head, DPGC convener, all faculty members, and the Department of Mechanical Engineering staff for their timely help and support. I am thankful to all the staff members of the **Mechanical Workshop** for their extended effort during the development of the test facility at IIT Indore

My heartfelt gratitude to my seniors, lab mates, and colleague researchers, especially **Mr. Prince Kaushik, Mr. Pawan Sharma, Mr. Pushpanjay Singh, Mr. Nishchay Saurabh, Mr. Dnyanesh Mirikar, Mr. Bhupendra, Mr. Rishabh Gupta, Mr. Janmejai Sharma, Mr. Nagendra Singh Ranawat, Mr. Vaibhav Hiwale** for their cooperation and stay to make MS (Research) journey happy and joyful.

I would like to offer special thanks to my parents, who have supported me in every step of my life since childhood. Their constant support and encouragement in my academic career from my school to my master's degree help me a lot to achieve my goals.

Finally, I am thankful to all who directly or indirectly contributed, helped, and supported me.

-Rahul Suryawanshi

Dedicated to my family for their love, care, and blessings

Abstract

The thesis deals with the average heat transfer characteristics of various orifice configurations and multi-orifice synthetic jet impingement on a heated flat plate. This study aimed to experimentally investigate the shape of the multi-orifice configurations (circular, elliptical, and mixed) to maximize the heat transfer rate at a given surface spacing. It is found that a single elliptical orifice exhibits better performance at lower surface spacing, whereas the single circular orifice outperforms the elliptical orifice at high surface spacing. These initial results motivate a combination of the elliptical and circular orifices in a multi-orifice configuration to optimize the heat transfer rate at a given surface spacing.

In this direction, four configurations of multi-elliptical and three configurations of mixed (combination of circular and elliptical) orifice are considered for the experiment. The maximum heat transfer is obtained with multiple elliptical configuration E-VC-(4H-4V)S (all elliptical (E) orifices having major axis vertical ellipse at the center(VC), 4 satellite (S) orifices having major Axis horizontal (4H) and other 4 having major Axis vertical (4V)) is 6% greater than that of SC (single circular orifice). Additionally, mixed configuration M-CC-(4C-4HE)S (mixed orifices (M) having a circular orifice at the center (CC), 4 circular satellite orifices (4C) and other 4 elliptical having major Axis horizontal (4HE)) consists of 15% higher heat transfer compared to SC configuration. The result indicates a strong correlation between orientation and the combination of satellite orifices in multi-orifice synthetic jet impingement heat transfer. The finding can be used for the thermal management of synthetic jet-based electronic equipment.

Keywords: *Multi-orifice, Synthetic jet, elliptical- orifice, Thermal management, Vibrating heated surface.*

List of Submitted Papers

Journals:

1. **R. Suryawanshi**, P. Sharma, P. Kaushik, S. Patel, S.K. Sahu, H. Yadav, “*Thermal characteristics of synthetic jet impingement with different multi-orifice configurations of circular and elliptical shapes.*” International Journal of Heat and Mass Transfer (2022), (Submission ID: HMT-D-22-02253)
2. P. Kaushik, **R. Suryawanshi**, P. Sharma, S. Patel, S.K. Sahu, H. Yadav, “*Flow resistance characteristics of fully developed turbulent pulsating flow in a circular pipe,*” Experimental Thermal and Fluid Sciences (2022), (Submission ID - ETFS-D-22-00706)

Table of Contents

Abstract	i
List of Submitted Papers	iii
Table of Contents	v
List of Figures	vii
List of Tables	ix
Nomenclature and Abbreviations	xi
1. Introduction.....	1
1.1. General background	1
1.2. Structure of SJ	2
1.3. Parameters influencing the formation of SJ	4
1.4. Applications of SJ	4
1.5. Brief literature review	7
1.6. Research gaps	10
2. Detailed Literature Review	13
2.1. Aspect Ratio	13
2.2. Orifice Shape.....	13
2.3. Orifice and Cavity dimensions.....	15
2.4. Dimensionless parameters.....	17
2.5. Jet-heated target spacing	17
2.6. Multi orifice.....	18
2.7. Effects of using a different type of target surface	20
3. Experimental Investigation and Data Processing	21
3.1. General background	21
3.2. Experimental setup.....	22
3.3. Mathematical formulation.....	27

4. Results and discussion	31
4.1. Flow characteristics of single and multiple orifice SJ.....	31
4.1.1. Flow characteristics of single orifice SJ	31
4.1.2. Flow characteristics of multiple orifice SJ	32
4.2. Heat transfer characteristics of single and multiple-orifice SJ.....	34
4.2.1. Comparison of single orifices (i.e., circular and elliptical)	34
4.2.2. Comparison of multiple orifices	35
4.2.2.1. Comparison of single circular and multi- circular orifice SJ...35	
4.2.2.2. Comparison of multi elliptical orifice SJ	35
4.2.2.3. Selection from multi elliptical orifice configurations	36
4.2.2.4. Mixed orifice configuration	37
4.2.2.5. Comparison of multi- elliptical and mixed configurations of orifice	38
5. Synthetic Jet Impingement on a Vibrating Heated Surface	41
5.1. General background	41
5.2. Experimental setup	42
5.3. Methodology	43
5.4. Results and discussion.....	43
6. Conclusions and the scope for future work.....	45
6.1. Conclusions	45
6.2. Scope of future work	46
References.....	47

List of Figures

Fig. 1.1 Structure of SJ	3
Fig. 1.2 Parameters influencing the formation of SJ.[20–22].....	4
Fig. 1.3 Proposed mixing device. (a) Schematic view of the device, (b) pumping mechanism at the nozzle.[25]	5
Fig. 1.4 Synthetic jet in the electronic device. [28]	6
Fig. 1.5 Flow vectoring representation caused by the synthetic jet.[29]	6
Fig. 1.6 SJAs’ installation in aero-foil (wing) model.[31].....	7
Fig. 2.1 Velocity alterations along the centerline of SJs [59].....	14
Fig. 2.2 Variation appearing in Nusselt number pertaining to jet-wall positioning for distinct orifice contours of the identical hydraulic diameter.[68].....	15
Fig. 2.3 Change in average velocity by excitation frequency for distinct orifice size and cavity heights. The orifice diameters are (a) 3 mm, (b) 5 mm, and (c) 8 mm.[72].....	16
Fig. 2.4 Radial dispersal of time-averaged Nusselt number for every H/D (i.e. 2, 4, 6, 8 and 10) at Re equal to 5250. (a) for $L_0/D = 20$ and (b) for $L_0/D =$ 10. [1].....	18
Fig. 2.5 Comparison of Nusselt number for a different number of satellite orifices and baseline cases. [2].....	19
Fig. 3.1 Schematic of the experimental setup for synthetic jet impingement heat transfer.	22
Fig. 3.2 Schematic of the investigational setup for velocity measurement.	24
Fig. 3.3 Different orifice configurations are considered in the present investigation.....	25
Fig. 3.4 Heat loss from the test surface with the temperature difference between the heated surface temperature (T_s) and the ambient temperature (T_a).	28
Fig. 4.1 effect of the excitation frequency on the average Re (Re_{avg}) (obtained by average jet velocity) at the exit of a single circular orifice.	31

Fig. 4.2 The jet centerline average velocity versus z/d for single circular (SC) and single elliptical (SE) orifice.	32
Fig. 4.3 power required as a function of frequency for (a) single orifice (circular and elliptical) and (b) a multi-orifice configuration. (c) Power required for various multi-orifice configurations at a resonance frequency (90 Hz).....	33
Fig. 4.4 Normalized centerline velocity as a function of z/d for different multiple-orifice configurations.	34
Fig. 4.5 Variation of Nu_{avg} for single circular and single elliptical orifice.	35
Fig. 4.6 Variation of Nu_{avg} for single and multi- circular orifice.	36
Fig. 4.7 Variation of Nu_{avg} for multi elliptical orifice configurations.....	37
Fig. 4.8 Comparison of Nu_{avg} for two best multi elliptical orifices with multiple circular orifice (C-CC-8S) configurations along with baseline configurations (single circular (EC) and single elliptical (SE)).	38
Fig. 4.9 Variation of Nu_{avg} as a function of Z/d for mixed configuration of orifices.	39
Fig. 4.10 Comparison of Nu_{avg} for multi-elliptical and mixed configuration..	39
Fig. 5.1 Schematic of the setup for heat transfer from a vibrating surface.....	42
Fig. 5.2 Effect on Nu_{avg} due to vibration exciter frequency at different z/d	43

List of Tables

Table 1: Specifications of different single and multi-orifice plates	25
Table 2: Description of the orifice configurations	26

Nomenclature and Abbreviations

d	Diameter of center orifice (mm)
d'	Diameter of circular satellite orifice (mm)
f	Diaphragm oscillation frequency (Hz)
H	Cavity depth (mm)
z	Axial distance between the heated copper block and orifice plate (mm)
z/d	Normalized axial distance
T	Period of diaphragm oscillation cycle (s)
t	Time (s)
U_o	Time-averaged jet blowing velocity over the entire cycle (m/s)
u	Instantaneous jet exit velocity (m/s)
x	Axial coordinate measured from the orifice exit (mm)
ν	Molecular kinematic viscosity (m ² /s)
T_s	Surface temperature (°C)
T_a	Ambient temperature (°C)
Nu_{avg}	Average Nusselt number
CJ	Continuous jet
SJ	Synthetic jet
SJA	Synthetic jet actuator
HWA	Hot wire anemometer
CTA	Constant temperature anemometer
AR	Aspect ratio
PCR	Pitch circle radius

Chapter 1

Introduction

1.1. General background

In the contemporary world, there is a huge requirement for electrical devices that has to be tiny in stature, occupy less system space, and provide maximum performance. As a result of excessive heat generation and the limited heat removal surface area, cooling electronic devices is now a substantial task. On the other hand, traditional cooling devices have some limitations and provide challenging problems for adequate cooling of future electronic equipment due to space restraints and the expectation of higher cooling loads. Further, technological advancements have significantly increased electronic devices like tablets, laptops, desktops (PCs), and mobile phones. Heat generation increases dramatically due to increased power density, which affects reliability and performance. Furthermore, carrying on a tablet PC with a surface temperature of 42 to 45 °C (on the rear side) has been shown to cause considerable user pain [3–5]. The life of an electronic device with flichips can be diminished by 4% with a 1 °C increase in operating temperature. In addition, a 10 °C to 20 °C increase in running a temperature can cause flichip electronic device failure [6]. In this situation, a suitable cooling technique for thermal control and proper functioning of electronic components must be established. Thermal challenges exist over distinct dissipation levels, from steep handheld devices to high-performance microprocessors radiating over the peak power density [7]. The power intemperance from high-functioning microprocessor chips is estimated to be around 360 W, as reported by International Electronics Manufacturing Initiative (iNEMI) Technology Roadmap [8]. In reality, the micro-and power-electronics sectors are tasked with removing an elevated heat flux of roughly 300 W/cm² though keeping the temperature below 85 °C [9]. Traditional cooling system includes thermosyphons [10], heat pipes [11], electro-osmotic pumps [12], microchannels [13,14], jet impinging [15], thermoelectric coolers [16], and absorption refrigeration systems [17] are used for these devices. These cooling techniques can be split up into two types: passive and active cooling systems.

In passive cooling systems working fluid circulates using capillary or gravity buoyancy forces, whereas active cooling systems use an external pump or compressor to enhance cooling capability and performance. Traditional systems need heat sinks that should be smooth and flat surfaces for better heat dissipation, which increases construction expenses. Further, the forced air cooling (fan) entails more space in the system; heat pipes are hollow metal pipes that only contain thermal liquid and could potentially cause harm [18]. To help relieve these restraints, synthetic jet (SJ) might be used for cooling functions. Impinging synthetic air jets can be used in many applications for cooling [19], such as electronics management, microprocessors and graphics processing units. Synthetic air jets are already explored and applied for fast-cooling requirements.

1.2. Structure of SJ

SJ is a novel approach for generating a jet from the fluid in which it is immersed. SJ relies on a fundamental principle one side of a partially enclosed chamber has a flexible membrane and an orifice opposite to the membrane, as shown in the Fig. 1.1. The membrane alternates as a result of an electric magnetic actuator diaphragm, forcing air/fluid in and out of the orifice on a routine basis. The jet pauses for an infinitesimal duration while moving through the sharp inner and outer edges of the orifice, resulting in the arising of the vortex. This results in forming a non-zero average stream-wise pulsing jet fore of the orifice, which may be directed against a heating surface to facilitate cooling using a diaphragm. A control system is used to move the diaphragm in time-harmonic motion. As the diaphragm pushes further into the cavity, the volume of the cavity reduces and fluid is evacuated from the opening. As fluid goes through the orifice, it separates at the sharp edges, resulting in vortex rings that roll up, forming vortices [20]. These vortices migrate outward as of the orifice's edges owing to their self-induced velocity. The entrainment of fresh fluid results in the expulsion of an earlier produced vortex due to its self-induced velocity and leads to the movement of the jet towards the heated target.

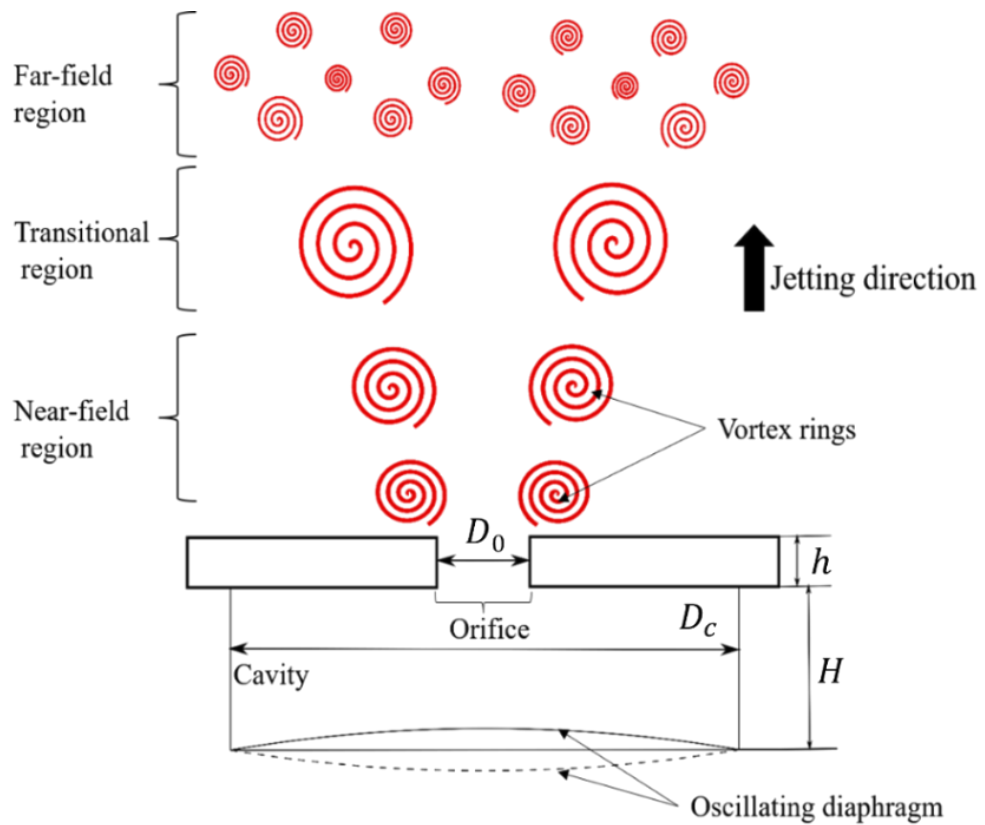


Fig. 1.1 Structure of SJ

If the cavity capacity is increased, then the ambient fluid is sucked in from a long-distance aperture. The ambient fluid entrained into the hollow does not influence the vortices because they have all been removed from the orifice's sidewalls [20]. As the vortices depart from the aperture, they entrain the ambient fluid and produce a jet of fluid. As a result, there is no net mass gain inside this procedure [21]. This characteristic negates the demand for sophisticated piping or packing in the system. Three regions in the direction of SJ flow based on the development of vortex rings are depicted in Fig. 1.1. The region near the orifice exit is termed a near-field region; due to the confinement of the jet in this region. The near-field has less mixing and hence less heat transfer. As vortices move further due to the self-induced velocity, they grow and become broader than that in the near-field region; this region is known as the transitional region. Further, as the jet moves beyond the transitional region, its velocity decreases; hence, the vortices vanish by mixing in the surrounding fluid.

1.3. Parameters influencing the formation of SJ

The characteristics of SJ-induced heat transfer and flow field working can be classified into three essential criteria: actuation parameters, geometrical factors, and fluid parameters (Fig. 1.2). In the case of SJ, discharging a pair of vortex rings or vortical structures at a low Reynolds number (Re) various dependent properties differentiate the production and evolution of the SJ for a specific system and operating conditions. Various parameters, as shown in Fig. 1.2, affect the flow and heat transfer characteristics of SJ. The frequency and amplitude of the synthetic jet actuator (SJA) regulate the velocity of the jet coming out from the orifice. Orifice specifications such as thickness, diameter, shape, etc., affect the formation of vortex rings. Mean velocity, viscosity and the temperature of the surrounding fluid are some fluid parameters that decide the heat transfer and flow behavior of SJ.

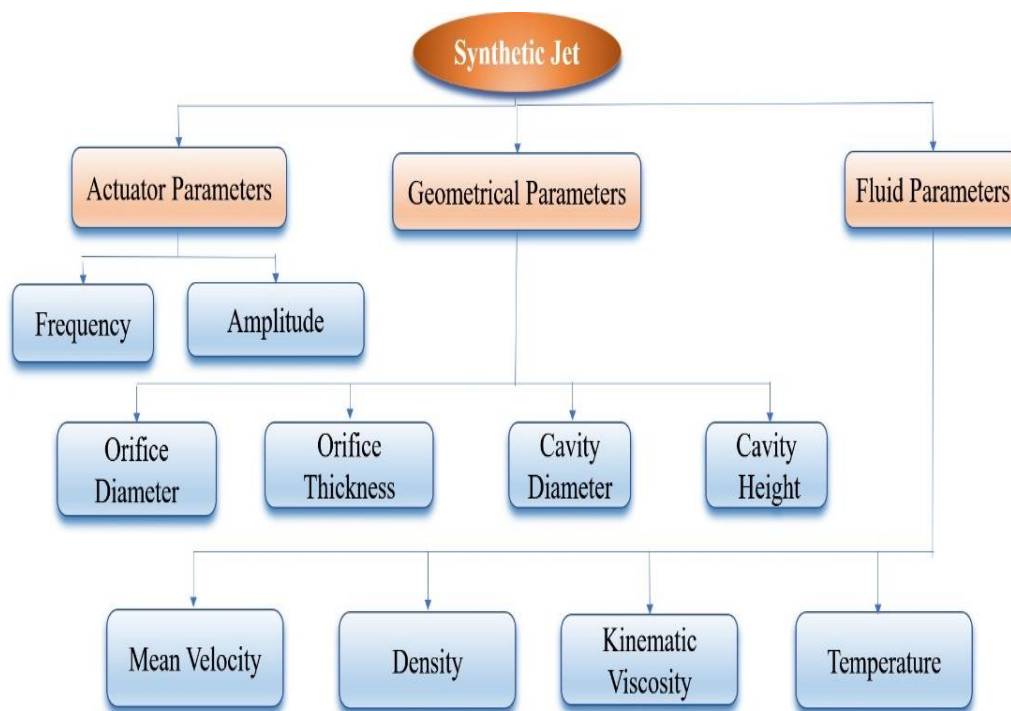


Fig. 1.2 Parameters are influencing the formation of SJ.[22–24]

1.4. Applications of SJ

Jet impingement is a widespread heat transfer technique for cooling, heating, or drying that includes high local heat transfer rates [25]. Jet impingement has recently gained popularity due to its numerous uses for high heat flux. Jet impingement is utilized for various applications.

- Mixing Purpose:** In various sectors, mixing is critical; thus, different strategies are proposed to reduce local shear rates in mechanically stirred mixing containers [26]. It is also known as continuously stirred tank reactors for mixing delicate materials such as biological and bio-fluids, where a high shear rate may harm the sensitive material [27]. Synthetic air jets can be used to mix the materials. The use of synthetic jets for mixing is a feasible alternative to traditional vessel-based mixing techniques [28]. Fig 1.3 illustrates L. Le Van et al. [25] proposed device, which does not require a valve to control flow. The experiment and subsequent simulation findings confirm the device's performance and attributes. The one-gate pump chamber and opposite inlet channels allow it to pump and mix the fluid simultaneously [27].

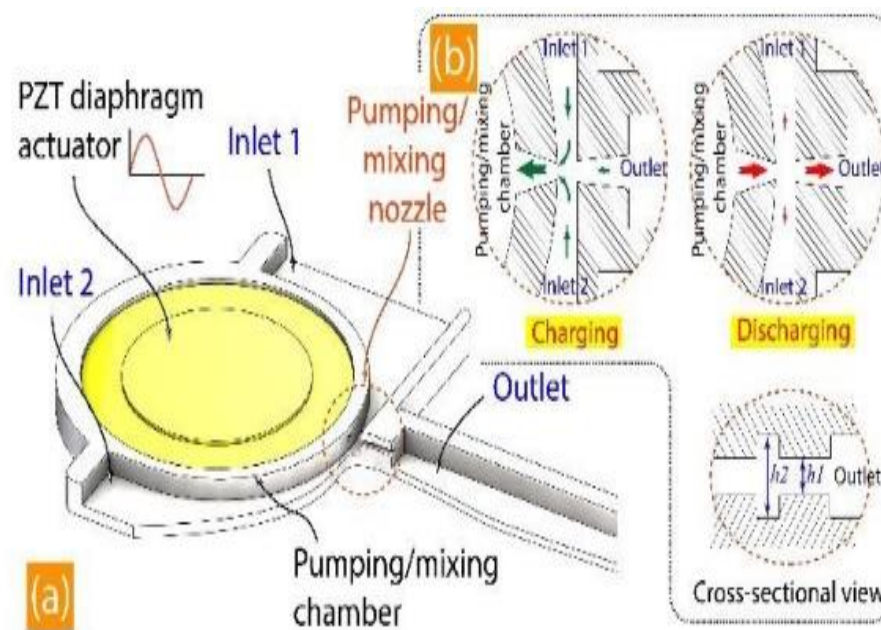


Fig. 1.3 Proposed mixing device. (a) Schematic view of the device, (b) pumping mechanism at the nozzle.[27]

- Electronic Cooling:** Electronic gadgets produce a large amount of heat, which causes thermal overstressing and electronic component failure [18]. The most crucial part of electrical system design is thermal regulation. Traditional cooling systems include heat sinks, forced air cooling and heat pipes. Heat sinks must have a soft and flat surface for improved heat indulgence, which increases manufacturing costs. However, forced air cooling (fan) demands more area in the structure; and heat pipes employ a hollow

metal tube transporting thermal liquid, increasing the chance of massive losses. The SJ can be used in various conditions, as shown in Fig. 1.4, because air has zero net mass fluid that can be sucked and evacuated for cooling [29].

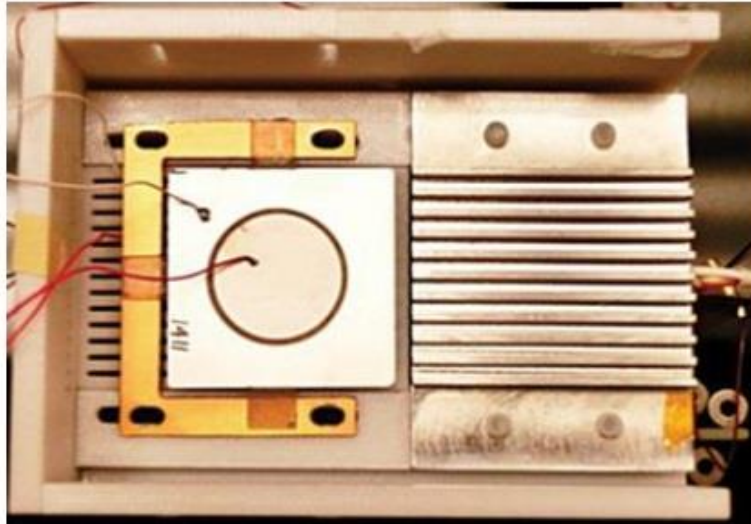


Fig. 1.4 Synthetic jet in the electronic device. [30]

- **Jet Vectoring:** Jet vectoring is the process of providing the direction of one jet using another jet, as depicted in Fig. 1.5. The primary air jet vectoring control system employs a unique SJA that vectors the primary jet by altering the position of the SJA's output point axially. This application may be used to improve thrust vectoring while lowering the thermal signature [31].

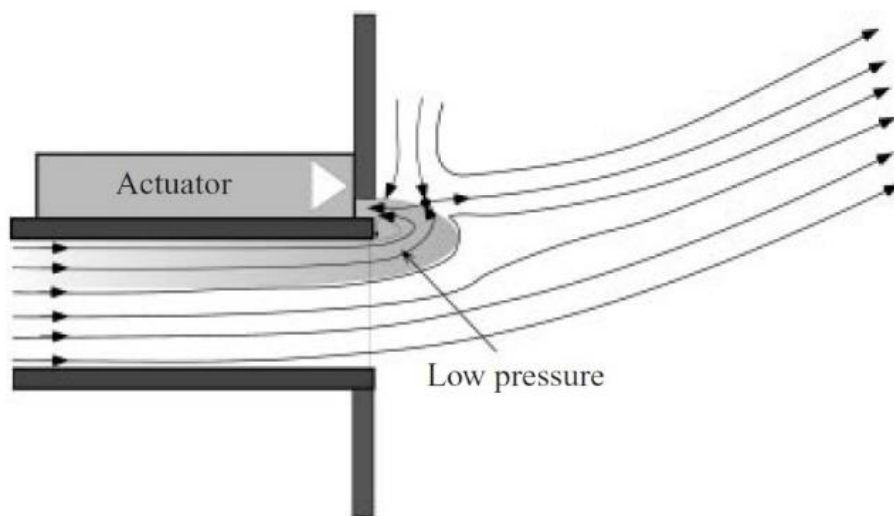


Fig. 1.5 Flow vectoring representation caused by the synthetic jet.[31]

In aeronautics, extensive research is being conducted to build aerospace vehicles that use synthetic air jets to regulate airflow in aircraft to improve lift coefficient, boost maneuverability, and minimize noise. SJ is used in aviation (as shown in Fig. 1.6) to assist with various issues such as weight, reaction time, force, flow control complexity and limit the amount of noise [32]. In the assembly shown in Fig. 1.6, the 1-in. full-range speaker units are designed as jet actuators, and three specific jet directions are achieved using different covers with varied jet angles [33]. The actuators are placed at 15% c (Actuator 1, A1) and 40% c (Actuator 2, A2) of the airfoil to control flow separation and increase the lift.

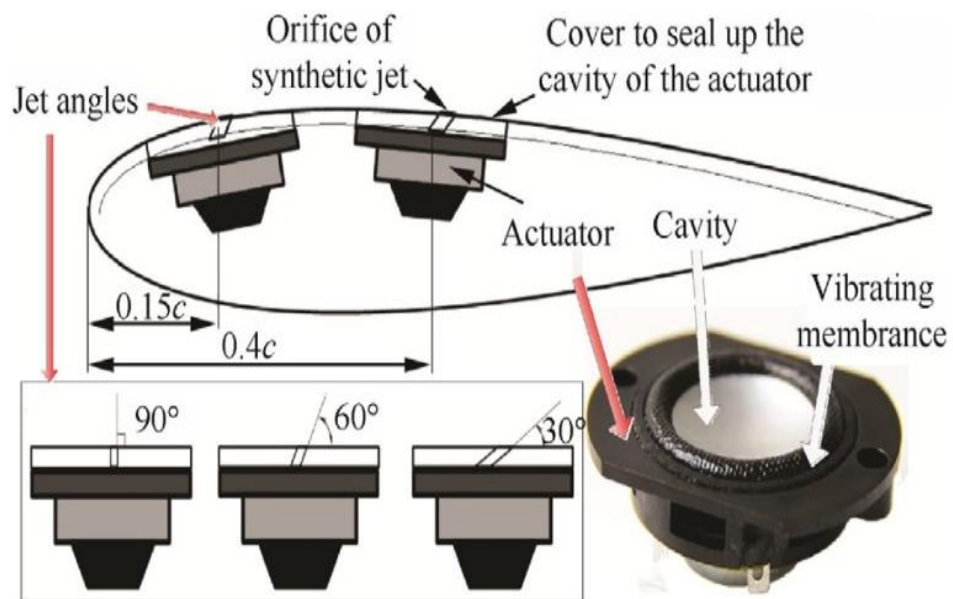


Fig. 1.6 SJAs' installation in aero-foil (wing) model.[33]

1.5. Brief literature review

The SJ is produced by pushing fluid consecutively into and evacuated from a tiny cavity by diaphragm motions before cavity [21]. As fluid passes through the orifice, it separates at the sharp edges, resulting in vortex rings that roll up, forming vortices [20]. These vortices migrate outward from the orifice's edges owing to their self-induced velocity. However, continuous jet (CJ) is generated by adding momentum and mass flow, whereas SJ is formed without mass addition. These are the critical characteristics of SJ that make it attractive for applications such as heat management of electronic devices, jet vectoring [31], flow separation control [33,34], turbulence mixing enhancement [28,35] and underwater jet propulsion [36].

Various parameters have already been analyzed to optimize the performance of SJ-based thermal management. In this regard, Chaudhari et al. [37] offered a dimensional assessment to assess the impact of several characteristics, including Re , z/d and the surface area of the test sample. For optimal heat transfer performance, the orifice and the target wall must be combined [38]. Further, it is found that an ideal spacing between a jet and a flat heated surface is needed when extreme heat is generated [1,38–49]. Hence, the heat transfer performance is mainly contingent on the location of the constant heat flux of flat plates [38]. The existence of the flat plate in the near-field limits the jet's skill to entrain cool ambient fluid. However, in the far-fields, diffusion reduces the jet velocity, consequent in a fall in blending and heat transfer rate.

The diaphragm's actuator parameters (frequency and amplitude) considerably influence the flow and heat transfer. Arun et al. [50] showed that the highest average Nusselt number increases by 40% when the frequency increases from 10 Hz to 50 Hz. Moreover, frequencies and average Nusselt number are expanded with the z/d ratio to a maximum value up to some extent and then drop subsequently. Further, Pavlova et al. [39] found that the optimal value of the z/d ratio diminishes as the frequency increases. On the other hand, the increased frequency of SJ forms vortex rings and breaks up into tinier structures before impinging on hot surfaces. In the case of lower SJ frequency, the separation between comprehensible forms is more significant and each vortex ring impinged on the heated surface independently. The 'vortex shedding' phenomenon is occurred at the upstream border and causes local flow disturbances[51]. Giachetti et al. [51] also established a relation for excitation frequency to measure the synthetic jet flow's penetration index.

Further, the SJ flow field has an array of vortex rings convect downstream and lacks the strength to expand at high St or a low value of L [52,53]. The impact of SJ on the hot surface radially results in the heat transfer close to the proximity of the stagnation point [48]. However, when it comes to heat transfer, enrichment reduces the issue of an increase in L or a lower Strouhal number (St) [48,54]. In the radial zones, things improve after a period of stagnation (wall-jet region) SJA begins ejecting extra particles after the

threshold L is exceeded. The fluid, after the development of a vortex ring for the duration of the ejection phase, the trailing jet intermingles with the vortex ring, widening it and causing it to expand; improving mixing [52,55].

In addition to operating parameters, geometrical characteristics impact SJ's thermal performance. Orifice plate thickness (t), orifice size, cavity depth (H), and orifice shapes are among them. It is reported that reducing orifice depth from 5 to 1.6 mm increases mean ejection velocity for the circular, square and rectangular orifices, which increases heat transfer rate intensity [37,56]. Further, it has been found that orifice configuration substantially impacts the heat transfer rate from the surface [56,57]. The circular, rectangular, and square are the most commonly investigated orifice configurations [56,58]. The highest velocity caused by the orifice having both sides rounded is 25% lesser than that of the sharp orifice. This is due to the additional fluid can be pulled from the rounded edges and lowering the vortex formation inside the orifice. Jain et al. [59] examined the effect of orifice and cavity parameters on the flow behavior of SJs using a bevel-shaped orifice. In another study, Bhapkar et al. [57] observed that for lower surface spacing ($z/d < 6$) elliptical orifice operates healthier than the other shapes. This is because of superior mixing and a significant entrainment rate due to the phenomenon known as axis switching [60,61]. Non-circular orifices (rectangular, elliptical) exhibit axis-switching of fluid. Because initially, the fluid is sucked about the larger Axis and expelled about the shorter Axis, which leads to the former's contraction and the latter's stretching [62]. However, for the larger surface spacing ($6 < z/d < 12$), the circular orifice shows a superior heat transfer rate than the other orifices (rectangular, elliptical and square). Recently, the multiple orifices in SJ have been used to improve heat transfer at low power [63]. In this condition, jet issued from satellite orifices gets scattered and ambient fluid entrainment increases. [61]. At a particular axial length (z/d), the jet issuing from the satellite orifice joins the jet coming from the center orifice [64]. Persoons et al. [65] stated that an interacting SJ shows a 90% increase in average heat transfer rate compared to a single jet. The ejected SJs are propelled in phase by many orifices, whereas merging vortex pairs results in a single broader and stronger potential core region with significant momentum

flux. Thus, higher overall heat transmission is achieved even at bigger orifice-to-surface spacings [63]. Smith et al. [21] and Persoons et al. [65], show that more than one SJ affects flow field and heat transmission characteristics. Mangate et al. [64] studied the multi-orifice design without the center orifice and discovered that all satellite orifices behave like independent jets. These separate jets result in less mixing and heat transfer than a multi-orifice design with a center orifice. The SJs from satellite orifices allow more surrounding fluid to interact with the center orifice, thus resulting in increased heat transport. Chaudhari et al. [2] experimented on various topologies with a central orifice surrounded by satellite orifices. They varied Re from 1000 to 2600 and normalized axial distance from 1 to 30 and found that the multi-orifice SJ exhibits 30% higher heat transfer than the single orifice SJ.

It is evident from the above discussion that the multiple-orifice SJ-based thermal management technique has better heat transfer capacity. In the previous work, multi-orifice SJ has the same center and satellite orifices shapes are considered. Hence, in the present work, the effect of elliptical and circular orifice shapes on heat transfer in impinging multi-orifice SJ is studied. Thus, several elliptical and circular orifices are investigated to maximize heat transport.

1.6. Research gaps

SJAs have much potential in heat transfer applications (especially in electronics cooling). However, SJ is superior than CJ in terms of features. The SJ's applications for curved surfaces are not thoroughly studied compared to CJ's. There are several studies on SJ for flow field regulation; nevertheless, the heat transmission characteristics of SJ are understudied. Some potential research gaps for the SJ impingement are as follows:

- Limited findings have been made on the impingement of SJ on other than flat surfaces.
- Flow and heat transfer performance of concave/convex target plates can be helpful for the thermal management of various electric gadgets. The thermal management of electric motors has not been studied.

- The curvature of concave/convex targets significantly affects jet recirculation; hence, the heat transfer is rarely examined.
- The impingement of synthetic jets with multiple orifices is hardly explored.
- Orientation and the configuration of multiple orifices substantially affect the flow and heat transport characteristics. Efforts should be made for such studies.

This study explores the effect of elliptical and circular orifice shapes on heat transmission from an impinging multi-orifice synthetic jet. The heat transfer coefficient and the required distance between the orifice and the heated surface (z/d) can be affected by the configuration of the orifice. Hence, several combinations of elliptical and circular orifices are investigated from a heat transport point of view. The velocity measurements were also done with hotwire anemometry to derive the conclusion for the different behavior of distinct orifice configurations. The structure of the thesis is as follows:

Chapter 1: This chapter briefly introduces a synthetic jet with various areas where it can be applied. A brief literature review is also reported and objectives are highlighted.

Chapter 2: This chapter elaborates on the effect of various parameters examined in previous research.

Chapter 3: Chapter three presents the experimental investigations of different configurations' flow and heat transmission properties in multi-orifice synthetic jet impingement. Here, efforts have been made to study the effect of the alignment of elliptical and circular orifices to get the optimum heat transmission.

Chapter 4: The obtained results are elaborated in detail.

Chapter 5: The effect of the vibration of a heated target plate on heat transfer characteristics in single-orifice synthetic jet impingement is reported.

Chapter 6: Conclusions from present experimental investigations are presented in this chapter. The scope of further research is also discussed.

Chapter 2

Detailed Literature Review

It is critical to comprehend SJ's flow characteristics to improve its cooling efficacies. Research has demonstrated that the SJ's functioning and flow-field are related/responsive to Re , jet-heated target surface gap, geometrical parameters and excitation frequency. Thus, the SJ's performance has been assessed using a variety of factors and parameters, which are detailed in this chapter.

2.1. Aspect Ratio

The SJA [67] based investigation is conducted to assess the influence of the orifice aspect ratio (AR) on the jet flow in a calm condition [60]. The jets ejected from orifices with ARs of 1, 5, 10, and 16 were contrasted, while the cavity geometry and orifice area remained unchanged. The findings revealed that the axis-switching behavior became more noticeable as the AR grew. Further, a constant diaphragm displacement boosting the AR resulted in a more significant jet exit velocity. Zhong et al. [62] found that as the AR increases, the boundary layer adjacent to the orifice has a more substantial percentage of the orifice, which causes an increase in the jet exit velocity for a constant exit area (i.e., obeying continuity). On the other hand, the vortex ring caused by low AR will go through a more intensive vortex relocation process to settle into a stable axisymmetric formation, resulting in a faster velocity deterioration rate. A circular orifice shows low axial velocity decay, as shown in Fig. 2.1, because of the secondary vortex trailing behind the primary vortex ring. This is due to the excess circulation that the primary vortices cannot suppress. Whereas rectangular orifices with AR 5, 10 and 15 showed relatively higher decay in the axial velocity due to axis switching.

2.2. Orifice Shape

Chaudhari et al. [58] studied heat removal performance by an impinging SJ with various orifice forms (circular, square, rectangular), then followed by diamond and oval-shaped orifices [68]. As shown in Fig. 2.2 the square orifice

showed better heat transfer when a smooth surface was in the far-field [57,58]. In the near-field, the oval-shaped orifice outperformed others [57]. The rapid axis change can be justified by the fact that modifications in orifice geometry in the azimuthal direction cause intermittent self-induction and various vortex formations [69,70].

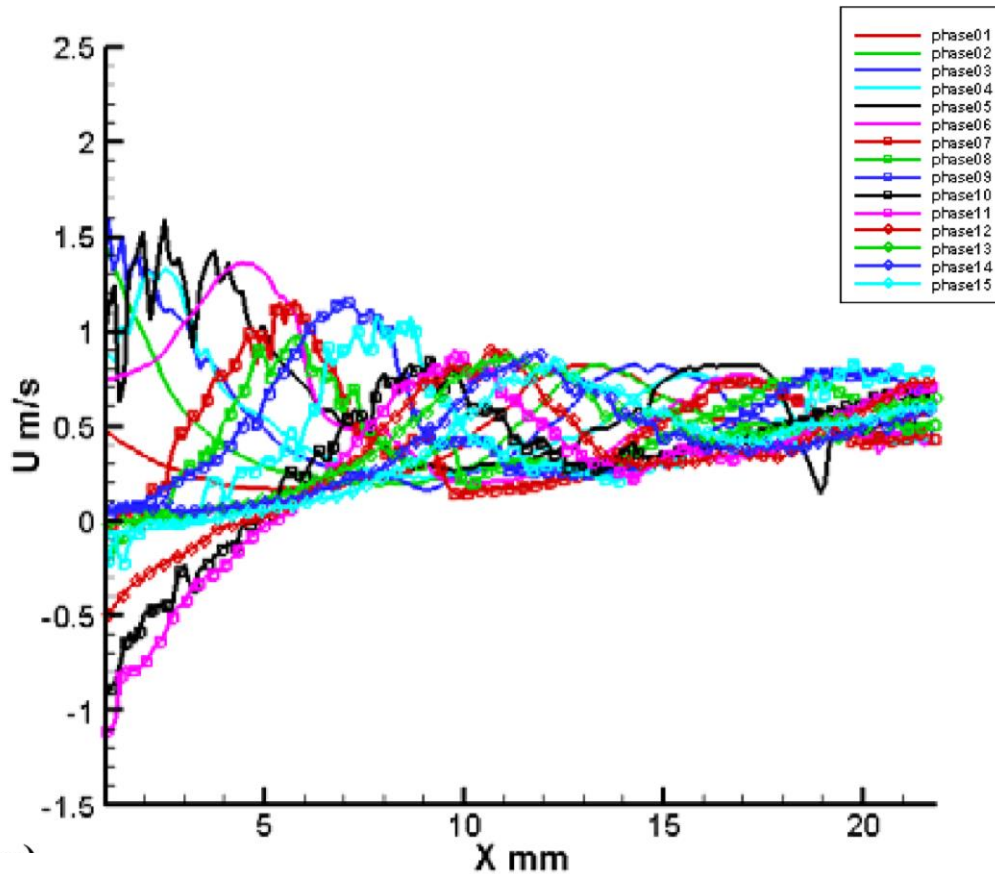


Fig. 2.1 Velocity alterations along the centerline of SJs [60]

As a result, the ring expands. After a series of contortions, the body moves quickly along the minor Axis. The Axis of the vortex ring is switched, but the ring regains its previous form [71]. The switching of the Axis, in turn, improves turbulence and entrainment of the ambient fluid. Heat transmission is improved due to increased intensity in the near-field at a very short axial distance.

Amongst all the shapes considered, square and rectangular orifices perform better in heat dissipation than all the shapes of the orifice for the entire range of axial distance, as illustrated in Fig. 2.2. However, oval and diamond shape

orifices perform better than circular orifices at lower axial distances. The higher value of average Nu for square and rectangular orifices can be attributed to the enhanced amount of entrainment[37]. It is understood that, due to this significant entrainment, these orifices attain a more considerable mass flux at the same distance from the heated surface.

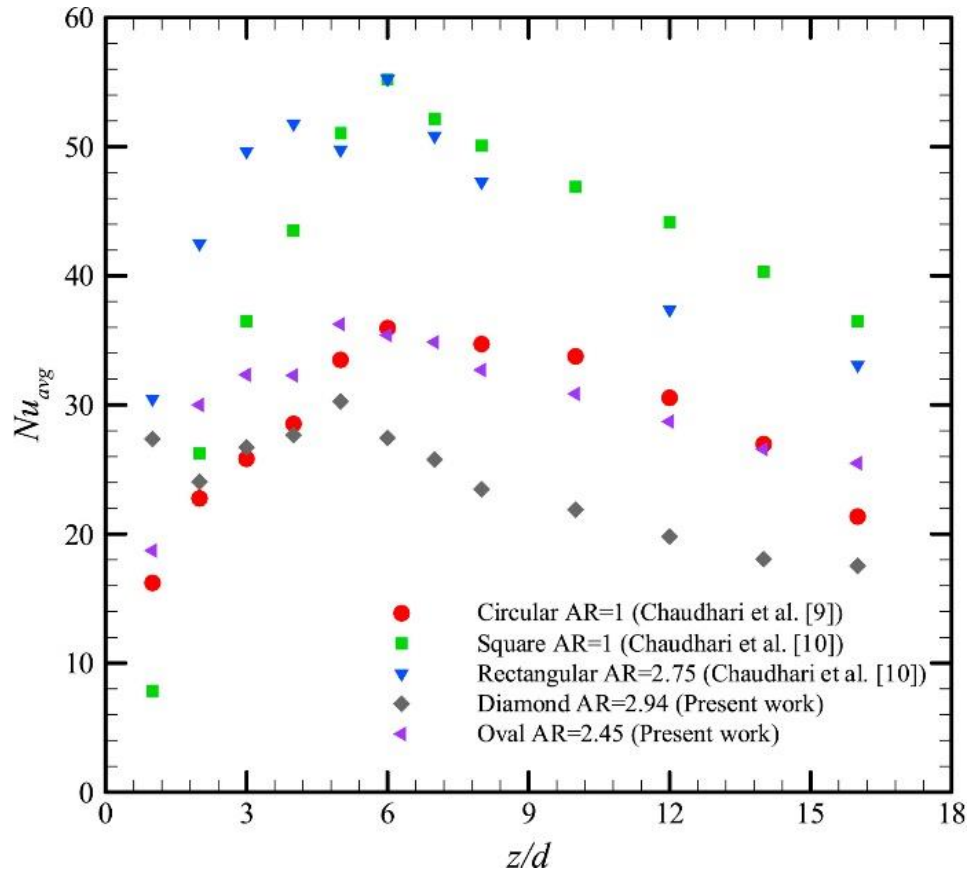


Fig. 2.2 Variation appearing in Nusselt number about jet-wall positioning for distinct orifice contours of the identical hydraulic diameter.[68]

2.3. Orifice and Cavity dimensions

In contrast to the findings [37,41], researchers claimed that cavity depth had no significant influence on SJ performance. Lee et al. [41] argued that a shallow cavity harms SJ performance and impacts average velocity. There may be a difference in outcomes attributed to the various dimensions and contours of orifices used for the investigation. Further, high average velocity does not have to be a need for good performance. They have also demonstrated that heat transfer performance SJ's abilities are not limited to D_h . Since SJ has a wide range of abilities, it underperforms when the velocity

is average, but the hydraulic diameter is small [41]. The orifice and cavity dimensions are significant in the SJA's performance. Typically, the SJ velocity vs. diaphragm excitation frequency graph will have two upper limits, as shown in Figs 2.3 (a) and 2.3 (b), or a single peak, as presented in Fig. 2.3(c). Despite the overall trend, Fig. 2.3 shows that the highest value varies from case to instance, indicating the importance of cavity and orifice sizes. For two reasons, consideration of orifice diameter was excluded. First, the orifice diameter is mainly defined by the thickness of the boundary layer. To keep flow disruptions minimum, boundary layer thickness should not be more than 5%. Second, the essential dimensionless parameters are calculated using the orifice diameter. As a result, it alters those factors and in most circumstances, the end effect will merely modify the Re.

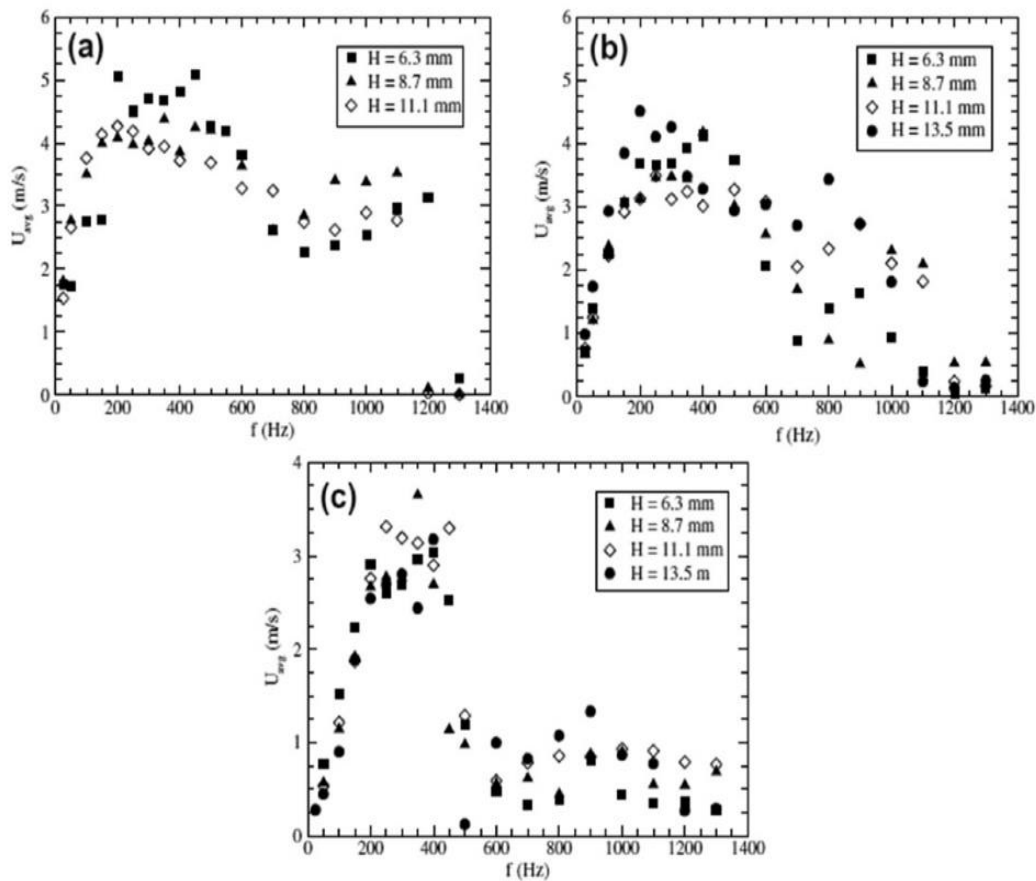


Fig. 2.3 Average velocity by excitation frequency for distinct orifice size and cavity heights. The orifice diameters are (a) 3 mm, (b) 5 mm, and (c) 8 mm.[72]

2.4. Dimensionless parameters

The stroke length refers to the distance of fluid vortex travels through the orifice during the SJ's ejection phase. The dimensionless stroke length is inversely related to the SJ's actuation frequency. The SJ flow field has a sequence of vortex rings that convect downstream and lacks the strength to expand at elevated St or a low value of L [52,53]. However, heat transfer enhancement reduces when an increase in L or a lower Strouhal number (St) [48,54]. In the radial zones, heat transfer increases after a period of stagnation (wall-jet region) due to SJA begins ejecting extra particles (above threshold L). The fluid develops a vortex ring throughout the ejection phase, drags jet interacts with the vortex ring, widens, expands, and improves mixing [52,55]. After impingement, the vortex structure is radially stretched out and develops in size and intensity. It rolls away down the flat surface and breaks into turbulence, increasing heat transmission with the length of dimensionless strokes. The originating fluid, i.e., $L \geq 16$, overtakes the vortex ring and begins to rotate, acting like a turbulent continuous jet [52,55].

The Re influences the spatial progression of near-wall vortex configurations of the impinging SJ. The vortex rings of SJs uphold coherence for a substantial distance after impingement against the wall for low $Re_{sj} = 166$. However, it loses coherence soon after impingement for high ($Re_{sj} = 664$, with no peak frequency

2.5. Jet-heated target spacing

Another dimensionless parameter has been proposed to recognize the dependency of heat transmission features on the space among the orifice and heated focus surface. In order to optimize heat transfer performance, the orifice and target wall must be combined [38]. It is found that an ideal spacing between a jet and a flat heated face is needed for maximum heat generation, as shown in Fig. 2.4 [1]. Fig. 2.4 (a) shows the radial Nu profiles for $L_o/D = 20$ and each nozzle-to-plate distance. At the shortest nozzle-to-plate distance, the time-averaged Nu distribution shows a plateau around the stagnation point ($r/D \leq 0.3$). Such a plateau corresponds to the region where the potential jet core impinges, over which the axial velocity profile remains constant [54]. Similar behavior is shown at $L_o/D = 10$ in Fig. 2.4 (b). At $H/D=2$, the plateau

region near the stagnation region is present, but it is less wide than that observed at $L_0/D = 20$ due to the limited extent of the potential-core-like region. Furthermore, the outer inflection point can be observed at similar radial positions for the shortest dimensionless nozzle-to-plate distances (i.e., r/D equal 1.6 and 1.9 for H/D equal 2 and 4, respectively). The heat transfer performance in these places largely depends on the location of the constant heat flux flat plate [1,38–49]. A flat plate in the near-field limits the jet's capability to tune cool ambient fluid. However, diffusion reduces the jet velocity in the far fields, causing a drop in mingling and heat transfer rate.

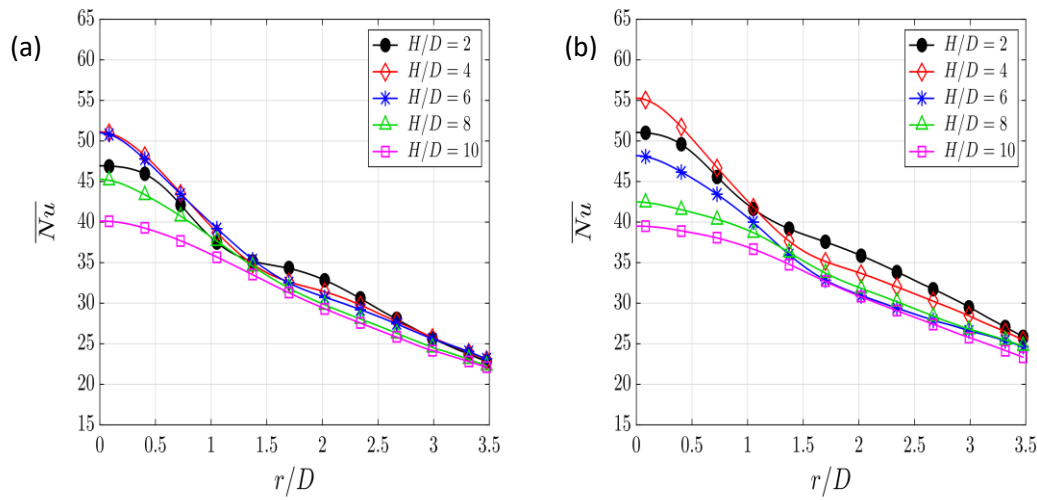


Fig. 2.4 Radial dispersal of time-averaged Nusselt number for every H/D (i.e., 2, 4, 6, 8 and 10) at Re equals 5250. (a) for $L_0/D = 20$ and (b) for $L_0/D = 10$. [1]

2.6. Multi orifice

The existence of beyond one SJ at a time alters the flow field and heat transmission [65,73]. The variation in the phase of the nearby SJ has a significant impact on the ejection's relative timing and the suction phase of nearby SJs owing to phase variation. There is a mismatch that influences the expelled vortex pairs. Numerous SJs are activated simultaneously; the vortex pairs are united [21]. It results in a single broader, more powerful vortex and higher momentum flux; thus, a more vital potential core region, even at large surface-jet sizes, increased overall heat transmission. Further, a unique movable slider mechanism is designed to control the vectoring of dual

synthetic jets (DSJ) [74]. This movable slider mechanism can adjust the phase angle also.

The spacing between neighboring SJs could be changed to regulate the DSJ's direction [2]. This is due to the consistent heat distribution in the adjustable DSJ. The heat transfer performance is better than the standard DSJ assigned to the impinging area and minimal region (wall-jet zone) of the vectoring DSJ's sweeping flow attributes [75]. The Chaudhari et al. [2] results in Fig. 2.5 reveal two peaks in the Nu versus axial gap. However, a different peak appears at reduced spacing with a particular number of orifices set at a specific pitch circle radius.

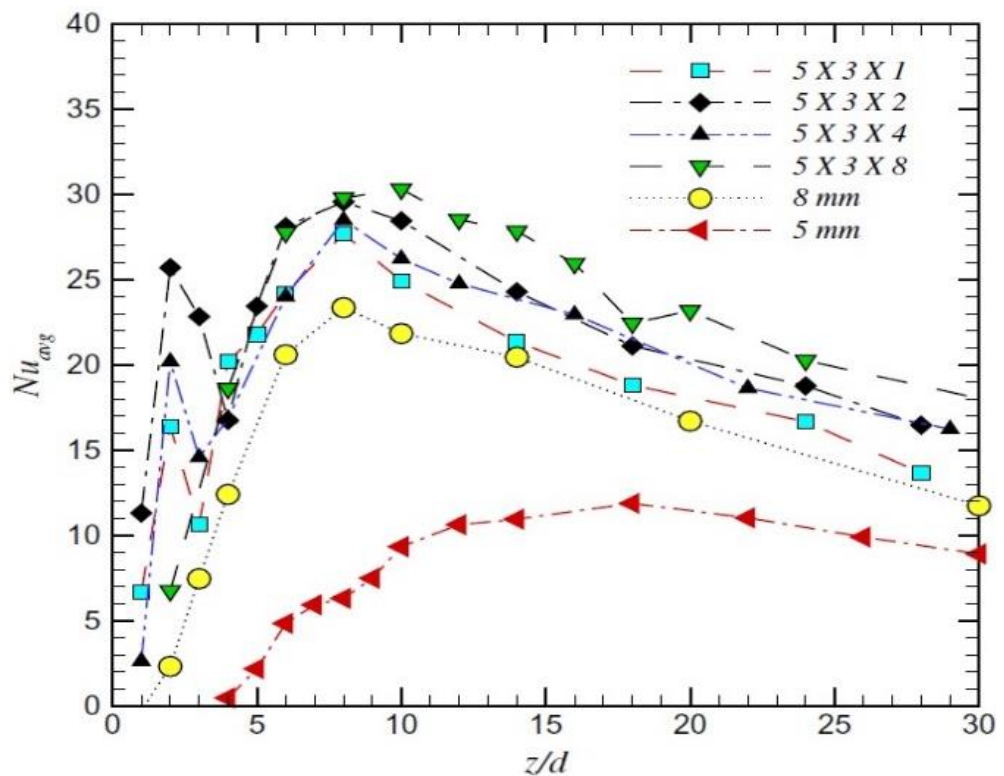


Fig. 2.5 Comparison of Nusselt number for a different number of satellite orifices and baseline cases. [2]

The heat transfer coefficient increases with the number of satellite orifices under considerable distances, but not at smaller spacing ($z < 15$ mm). An interesting observation is the presence of second maxima at small z , which appears with 1, 2 and 4 satellite orifices but not for 8 satellite orifices, as represented in Fig. 2.5. The magnitude of this second maxima increases with

the number of satellite orifices. Notice that there is a sharp increase at minimal spacing, followed by a sharp decrease in the average heat transfer coefficient near the first maximum; on either side of the second maxima, the decline is gentler.

2.7. Effects of using a different type of target surface

Section 2.1-2.6 contributed to the heat transfer characteristics and features of jet impingement on a flat sheet. Further, jet impingement heat transmission on a concave surface is desired for specific purposes, such as cooling gas turbine blades. Metzger et al. [76] studied a single string of circular jets impinging on a bowl-shaped cylindrical exterior in an experimental context. Re varied from 1150 to 5500, the H/d of 3-5 have maximum heat transfer [76]. As the Re grows, the ideal H/d value decreases. The average heat transfer levels for impingement on the concave surface were substantially higher than those on the flat plate, which was attributable to the curvature effect. Lee et al. [77] investigated the influence of concave side curvature on round impinging jets. They found that Nusselt numbers increased at the stagnation position and the wall jet territory as surface curvature. Fenot et al. [78] used infrared thermography to measure the 3D temperature dispersal of a concave semi-cylindrical surface. The concavity effect could enhance heat transmission, similar to Lee et al. [77] and Gau et al. [79]. Lyu et al. [80] studied single-row chevron-jet impingement heat transfer concave surfaces at different curvatures. They found that the concave curvature significantly impacts chevron-nozzle jet impingement heat transfer and is relevant to the Re of the jet and impinging distance.

Chapter 3

Experimental Investigation and Data Processing

3.1. General background

Multiple-orifice synthetic jet impingement for heat transfer is in its early stages of development. SJ multi-orifice configuration acts like an individual jet orifice. Still, a jet from satellite orifices gets combined with the center orifice at some distance in the near-field region to form a wider single jet with more strength in SJ. Bhapkar et al. [57] found that at lower surface spacing, the elliptical orifice performs better than the circular orifice. However, the circular orifice outperforms the elliptical orifice at higher surface spacing. This is an effect of Axis switching in non-circular orifices. The non-circular orifices surrounding fluid enter the major Axis and expel along the minor Axis. This is due to the stretching of the minor Axis and contraction of the major Axis. This phenomenon is known as axis switching and enables better mixing of the jet with the surrounding fluid, which may lead to more heat transfer in the near-field region. The above observation generates an idea of circular and elliptical orifices' simultaneous use in multi-orifice configurations.

The maximum heat transfer coefficient with a multiple orifice synthetic jet is approximately 12 times that of the natural heat transfer coefficient and up to 30% more than that obtained with a conventional single orifice jet. Interestingly, the average Nu gets maximized at two axial distances-the two peaks can be of comparable magnitude. The appearance, location and magnitude of the two peaks depend on the number of satellite orifices and the pitch circle radius on which the satellite holes lie. The input power reduces slightly in the multi-orifice case concerning the conventional design. The average velocity at the surface is also obtained with the help of hotwire anemometry. The use of multiple orifice synthetic jet does not appear to have been explored widely earlier and the results are expected to be helpful in several practical applications.

This chapter discusses the experimental result of different circular and elliptical orifices combinations in multi-orifice SJ impingement cooling.

3.2. Experimental setup

The schematic diagram of the experimental setup is shown in Fig. 3.1. A copper block of dimensions 40 mm × 40 mm and 5 mm thick is used as a test surface, as depicted in Fig. 3.1. The copper block is tightly fitted in an acrylic sheet of 5 mm thickness. The nichrome heater is placed underneath the copper block whose top surface is in contact with it. However, the bottom surface is adequately insulated with the help of glass wool and a bakelite sheet. The glass wool is also covered with aluminum foil for better insulation. Two pre-calibrated K-type thermocouples measure the average temperature of the copper block.

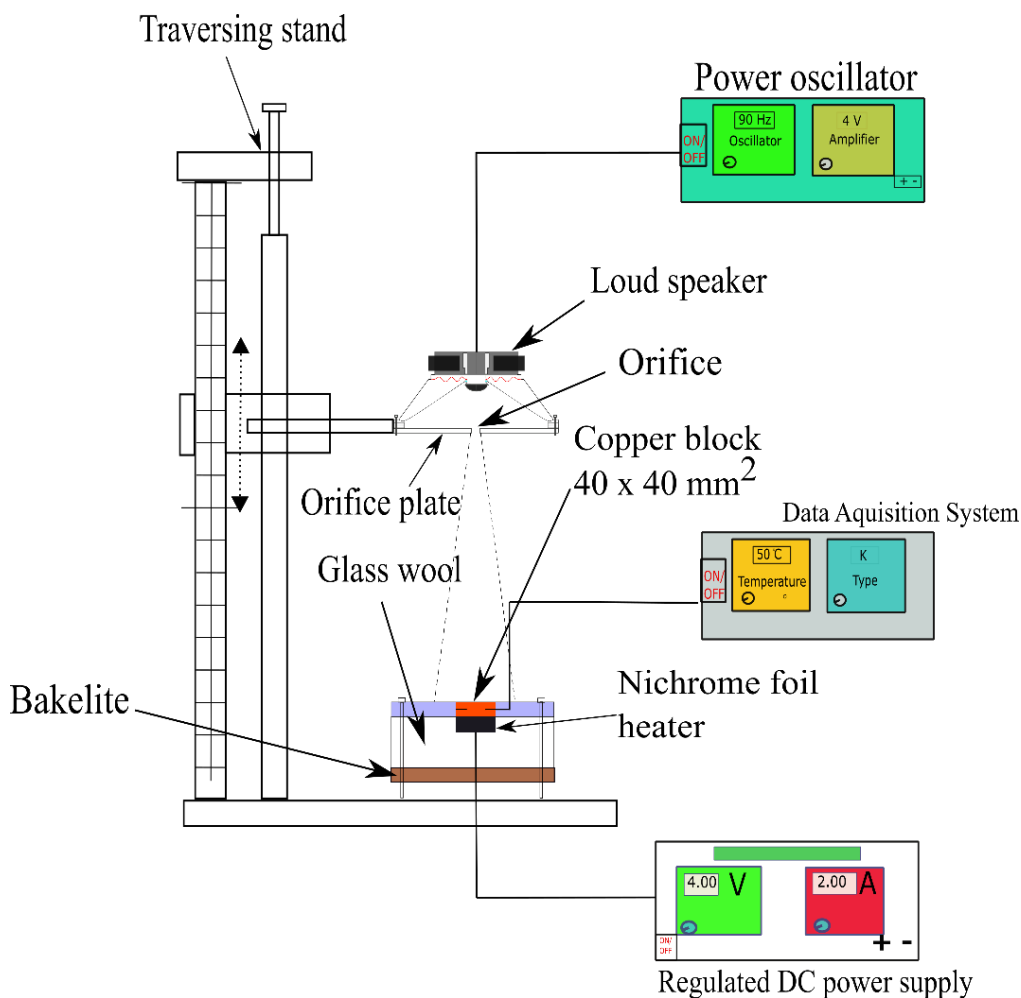


Fig. 3.1 Experimental setup schematic for synthetic jet impingement for heat transfer.

The 1 mm, diameter thermocouple bead is inserted into 10 mm deep holes of the copper block on both sides. The direct current (DC) power source (CROWN 0-12V/60 A) is used to heat the test specimen copper block. The current source and voltage drop across the copper block are determined by using a digital multimeter (Fluke: 15B+). In order to diminish the inaccuracy in temperature measurements, the minimum temperature variation between the heated surface and the ambient temperature is kept above 15 °C for all conditions.

A 3-D traversing stand, SJ actuator assembly, test surface, DC power supply, power oscillator, a constant temperature anemometer (CTA), and K-type thermocouples constitute the experimental setup, as shown in Fig. 3.1. The SJ is formed by an electromagnetic actuator (Visaton: FRS 8) with a diaphragm diameter of 71 mm, the resonance frequency of 90 Hz and a nominal impedance of 8 Ω . The orifice plate is made of transparent acrylic sheet and fastened with the help of 4 mm bolts. A silicon sheet is inserted beneath the depth plate to prevent air leakage between the acrylic sheet and the actuator. The 3-D traversing stand regulates the orifice test surface spacing (z). The traversing mechanism holds the aligning of an SJ assembly from a heated test copper block with an accuracy of 0.1 mm.

Constant power is supplied to the SJ actuator (speaker) by a power oscillator (Syscon Instruments: SI28-DR). The unit consists of a tunable sine wave oscillator and a power amplifier to inject current into the exciter coil of the electromagnetic actuator. The excitation frequency and applied voltage (amplitude) to the speaker can be altered according to the requisite. The present study maintains a sinusoidal wave signal with an amplitude of 4 V_{rms} as an input signal to the acoustic actuator. All the experiments are conducted at the diaphragm resonance frequency. A constant temperature anemometer (CTA) (Dantec Dynamics: Mini CTA 54T42, temperature coefficient of resistance = 0.0036/°C) with a 55P16 single wire probe having tungsten-platinum coating is used for the velocity measurement, shown in Fig. 3.2. The anemometer probe traversed on a 3-D navigating stand, allowing the aligning of the probe with an accuracy of 0.1 mm. The velocity of the fluid at a fixed

distance of 1 mm from the orifice is measured along with the various radial locations in the jet.

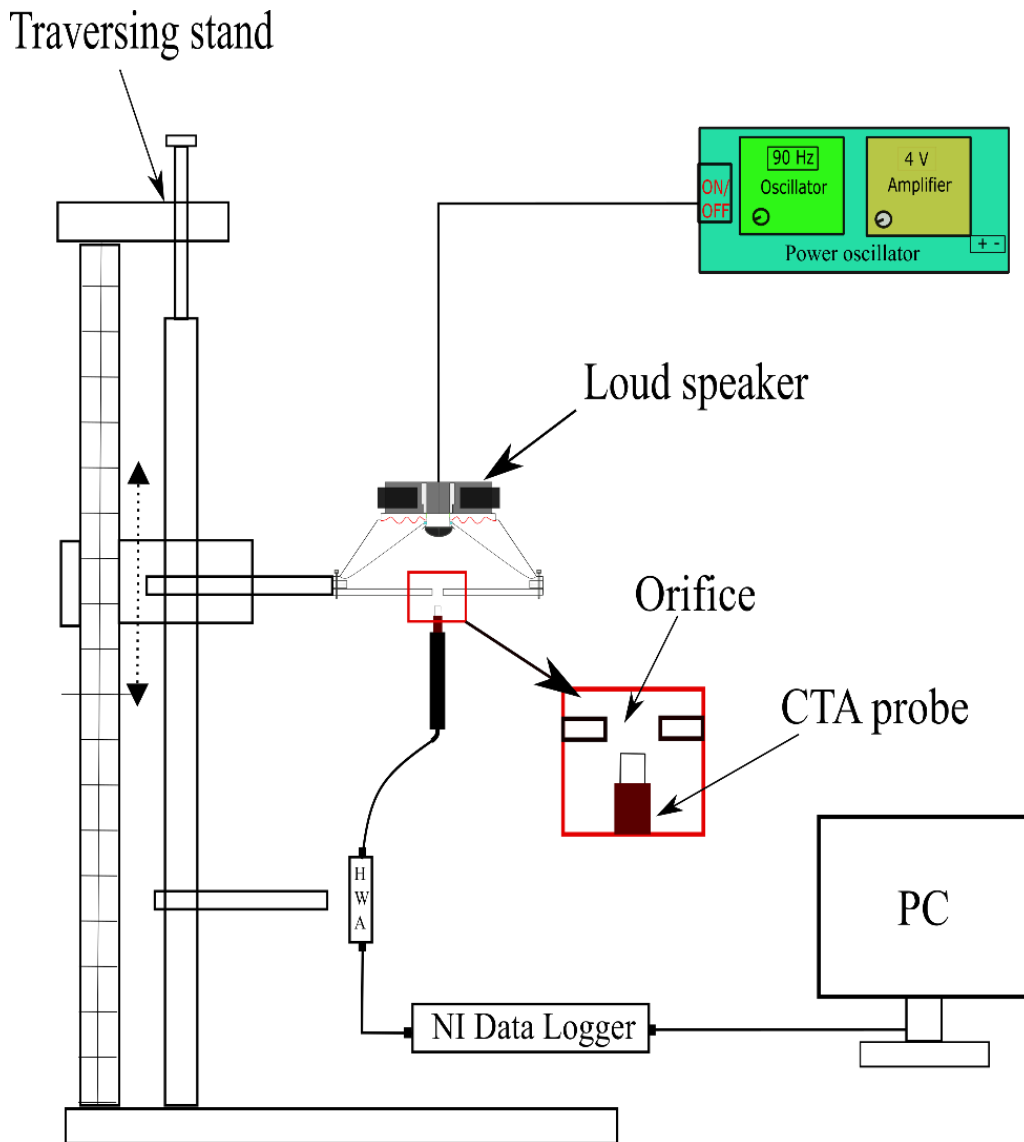


Fig. 3.2 Schematic of the velocity measurement setup.

The heat transfer and flow characteristics are investigated at different multi-orifice configurations. The effect of satellite orifices on Nu_{avg} is differentiated up to the pitch ratio ≤ 1.25 [64]. Beyond that, satellite orifices' SJ is combined with a center orifice to get a single jet. Thus, the pitch ratio of 1.5 (pitch circle radius = 7.5 mm) is chosen for all the multi-orifice configurations. The different single and multi-orifice configurations used for the study are illustrated in Fig. 3.3. Their specifications/dimensions are given in 1 and described in table 2.

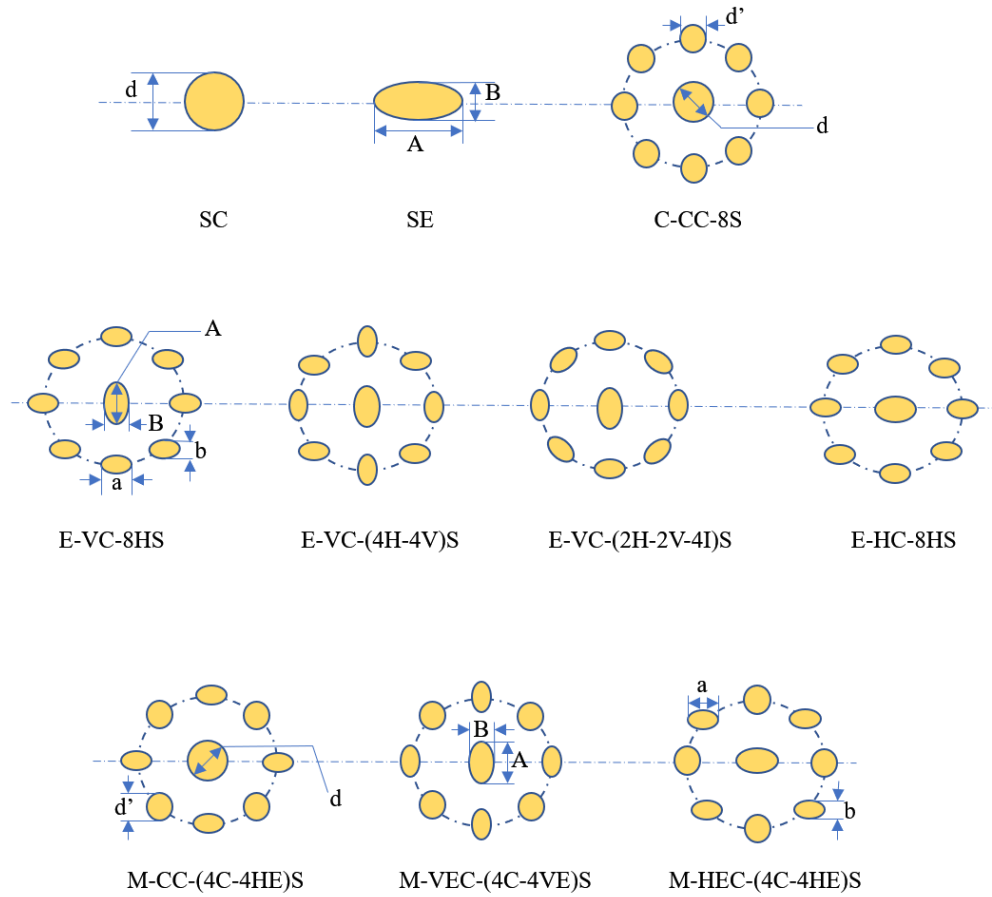


Fig. 3.3 Different orifice configurations are considered in this work.

Table 1: Specifications of different single and multi-orifice plates.

Orifice	Shape	Dimensions (in mm)
single orifice		
SC (Aspect ratio=1)	Circular	$d = 10$ mm
SE (Aspect ratio=2)	Elliptical	$A = 14.14$ mm, $B = 7.07$ mm
multi-orifice		
C-CC-8S	Circular	$d = 5$, $d' = 3.06$
E-VC-8-HS	Elliptical	$A = 7.06$, $B = 3.54$; $a = 4.33$, $b = 2.17$; A.R. = 2
E-VC-8-HS		
E-VC-(4H-4V)S		
E-VC-(2H-2V-2I)S		
M-VEC-(4C-4VE)S	Mixed	$A = 7.06$, $B = 3.54$; $a = 4.33$, $b = 2.17$; A.R. = 2; $d = 5$, $d' = 3.06$
M-HEC-(4C-4HE)S		
M-CC-(4C-4HE)S		

Table 2: Description of the single and multi-orifice configurations.

Orifice configurations	
Single orifice	
SC	Single circular
SE	Single Elliptical
Multi-orifice	
C-CC-8S	All orifices are circular, having eight satellite orifices.
E-VC-8-HS	All elliptical orifices have a major axis vertical ellipse at the center and eight satellite orifices have a major Axis horizontal.
E-HC-8-HS	All elliptical orifices have a major axis horizontal ellipse at the center and eight satellite orifices have a major Axis horizontal.
E-VC-(4H-4V)S	All elliptical orifices have a major axis vertical ellipse at the center, four satellite orifices have a major Axis horizontal and the other four have a major Axis vertical.
E-VC-(2H-2V-4I)S	All elliptical orifices have a major axis vertical ellipse at the center, two satellite orifices having a major Axis vertical, two satellite orifices having a major Axis horizontal and the other 4 inclined at 45°.
M-VEC-(4C-4VE)S	Mixed orifices have a major axis vertical ellipse at the center, four circular satellite orifices and the other four ellipticals have a major Axis vertical.
M-HEC-(4C-4HE)S	Mixed orifices have a major axis horizontal ellipse at the center, <i>four</i> circular satellite orifices and the other four ellipticals have a major Axis horizontal.
M-CC-(4C-4HE)S	Mixed orifices have a circular orifice at the center, four circular satellite orifices and the other four ellipticals have a major Axis horizontal.

3.3. Mathematical formulation

The time-averaged centerline exit velocity is resolved by integrating the instantaneous stream-wise velocity at nozzle exit over the expulsion phase (half of one entire cycle) [81] and it is calculated as

$$U_0 = \frac{1}{T} \int_0^{T/2} u(t) dt \quad (3.1)$$

The Re of the synthetic jet is determined as [21]

$$Re = \frac{U_0 \cdot d}{\nu} \quad (3.2)$$

where d_h and ν are the orifice hydraulic diameter and the kinematic viscosity of the fluid, i.e., air, respectively. Here, U_0 denotes the average velocity at the centerline and exit of the orifice for the ejection part of the cycle. It is calculated as [21]

$$U_0 = L_0 \cdot f \quad (3.3)$$

where f and L_0 denote the excitation frequency and the stroke length, respectively. Here, L_0 is estimated as [82]

$$L_0 = \int_0^{T/2} u(t) dt \quad (3.4)$$

where $u(t)$ denotes the instantaneous velocity measured during experiments. The Nu_{avg} is the ratio of heat transferred by convection to the heat transferred by conduction. It shows how much heat is transferred due to fluid motion as compared to the heat transferred by fluid via conduction and is calculated as follows

$$Nu_{avg} = \frac{h_{avg} \cdot d}{k} \quad (3.5)$$

where k denotes the thermal conductivity of air. The heat transfer coefficient (h_{avg}) can be estimated as

$$h_{avg} = \frac{q_{conv}}{(T_s - T_a)} \quad (3.6)$$

here T_s and T_a are the exterior temperatures of copper block and atmospheric temperature, respectively and q_{conv} shows the net heat convected from the surface of the copper plate to the air and that can be written as

$$q_{conv} = q_j - q_{loss} \quad (3.7)$$

here q_j and q_{loss} show the heat flux delivered to the copper block and heat lost to the environment, respectively.

q_j can be estimated from the voltage drop (V) across the test surface by measuring current (I) and the cooling surface area of the test specimen as discussed below

$$q_j = \frac{V \cdot I}{A} \quad (3.8)$$

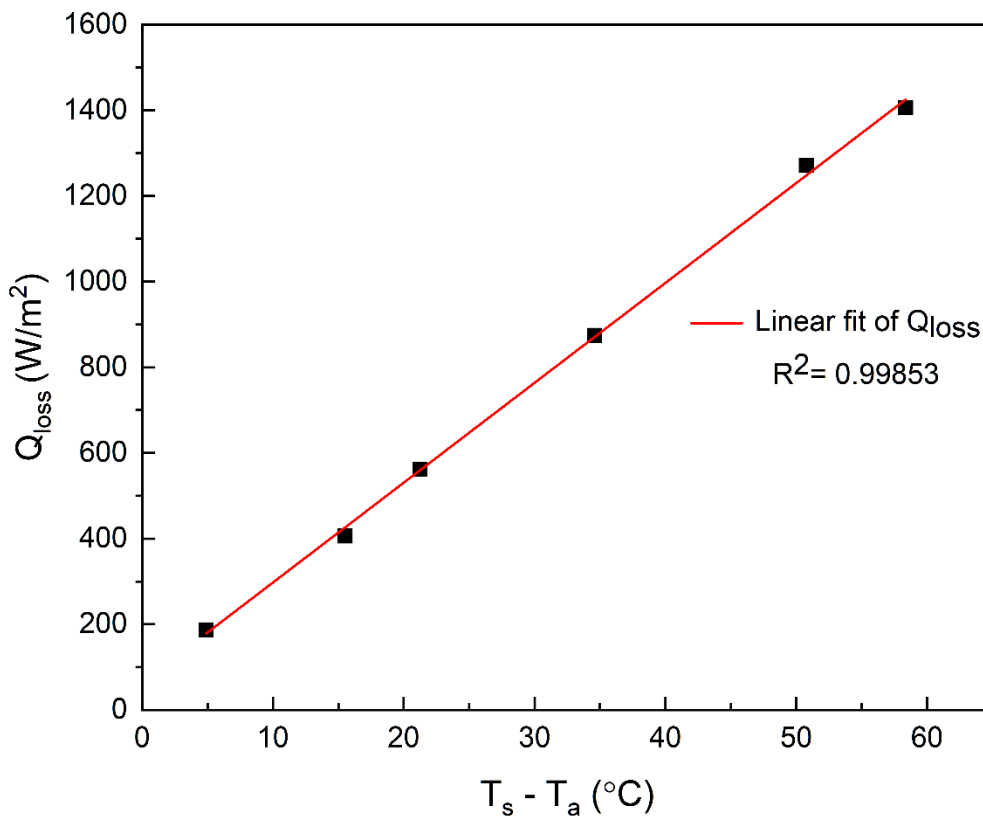


Fig. 3.4 Heat loss from the test surface with the temperature difference between the heated surface temperature (T_s) and the ambient temperature (T_a).

The heat loss computed depends on the temperature difference between the heated surface test foil temperature (T_s) and the atmospheric temperature (T_a). The heat loss calculation procedure is based on reference [83], where the no-

flow experiment calculates heat loss on thin foil. This method was also earlier followed by [57] for the heat loss calculation. Here, the heat loss from the targeted test surface is obtained by experimenting without an air jet impingement on the targeted surface. In this computation, a known electrical power was supplied to the heater and the surface temperature was recorded. Based on the temperature difference ($T_s - T_a$) and the supplied corresponding electrical power, a linear curve fitting will give a correlation for the heat loss from the test surface in terms of the temperature difference between the target surface and ambient temperature. The heat loss curve is shown in Fig. 3.4 and the obtained correlation for heat loss is as

$$Q_{loss} = 23.327 (T_s - T_a) + 64.283 \quad (3.9)$$

The heat loss is processed to be a maximum of 13% of the heat provided, including adding heat energy lost owing to natural convection and radiation on the top side of the heated test surface.

Chapter 4

Results and discussion

4.1. Flow characteristics of single and multiple orifice SJ

4.1.1. Flow characteristics of single orifice SJ

The SJA has a threshold frequency at which the jet orifice obtains maximum velocity and is termed resonance frequency. The resonance frequency is found at a specific voltage and particular amplitude (V_{rms}). In order to find the resonance frequency, the centerline velocity at the exit is measured for the single circular orifice (diameter 10 mm) using a CTA. The velocity is measured at the different frequency range from 25 Hz to 200 Hz and utilized to estimate the Re_{avg} , as illustrated in Fig. 4.1. It is found that at 90 Hz the Re of ejection cycles is maximum, as shown in Fig. 4.1. Thus, the resonance frequency of the speaker (90 Hz) is used for investigation. All experiments were carried out on it.

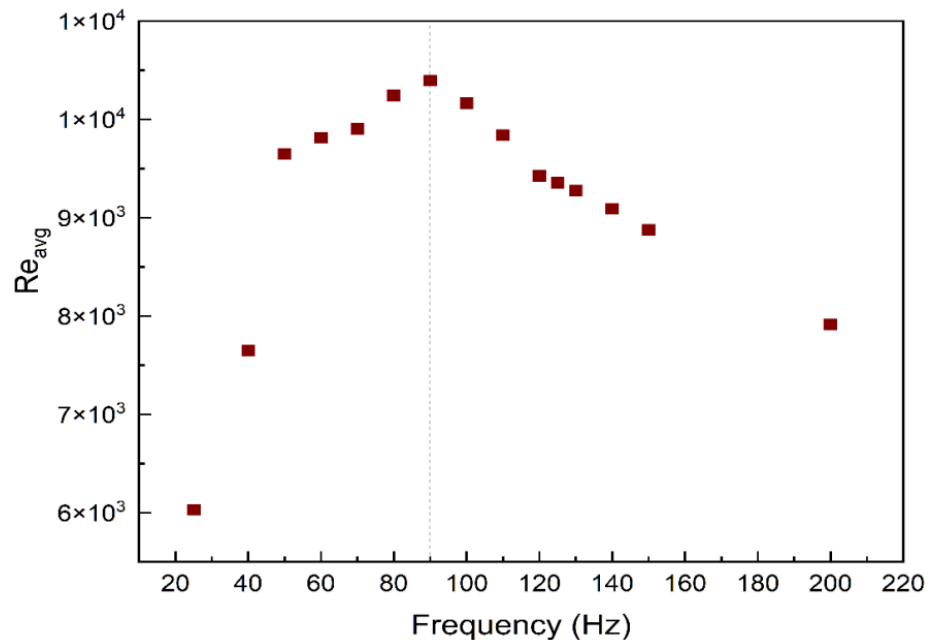


Fig. 4.1 effect of the excitation frequency on the average Re (Re_{avg}) (obtained by average jet velocity) at the exit of a single circular orifice.

The Fig. 4.2 shows the centerline jet velocity of single circular (SC) and single elliptical (SE) orifices as a function of z/d . It shows that SC and SE velocity is

almost the same concerning axial distance. Hence, the heat transfer from SJ issued from the EC orifice would be more at lower z/d because of axis switching. However, less heat transfer was obtained in the far-field due to comparatively more jet spreading. In the near field, the SJ is dominated by vortex pairs which permit more turbulence than in the far-field, where SJ resembles a continuous jet. Therefore, merging other vortices controls the fluid dynamics and heat transfer incidents.

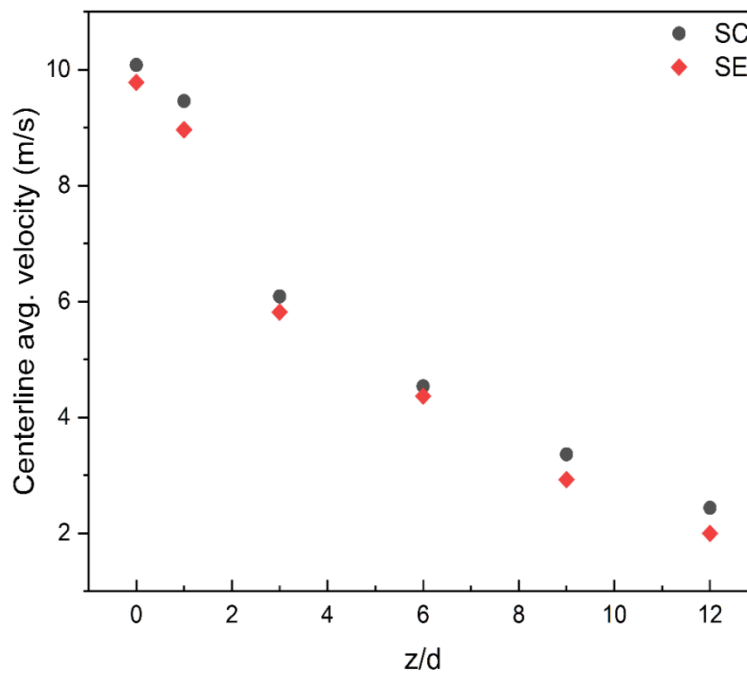


Fig. 4.2 The jet centerline average velocity versus z/d for single circular (SC) and single elliptical (SE) orifice.

4.1.2. Flow characteristics of multiple orifice SJ

Section 4.1.1 described the single orifice and maximum jet velocity found at the resonance frequency. However, multiple orifice SJs have some different characteristics compared to single orifice. In this direction, Fig. 4.3 depicts the power requirement for different orifice shapes. Fig. 4.3 (a) presents that the SC and SE require almost the same power at all frequencies and a minimum in the resonance frequency's vicinity (~ 90 Hz). Fig. 4.3 (b) shows the power variation for a multi-orifice configuration M-CC-(4C-4HE)S. The power distribution is similar to single orifices, which reveals that the shape of the orifice and the configuration (single or multiple) do not affect the power

required of SJA. Fig. 4.3(c) shows power consumption for different multiple-orifice shapes. It can be said that different multiple-orifice configurations require almost the same power, which is minimum at the resonance frequency.

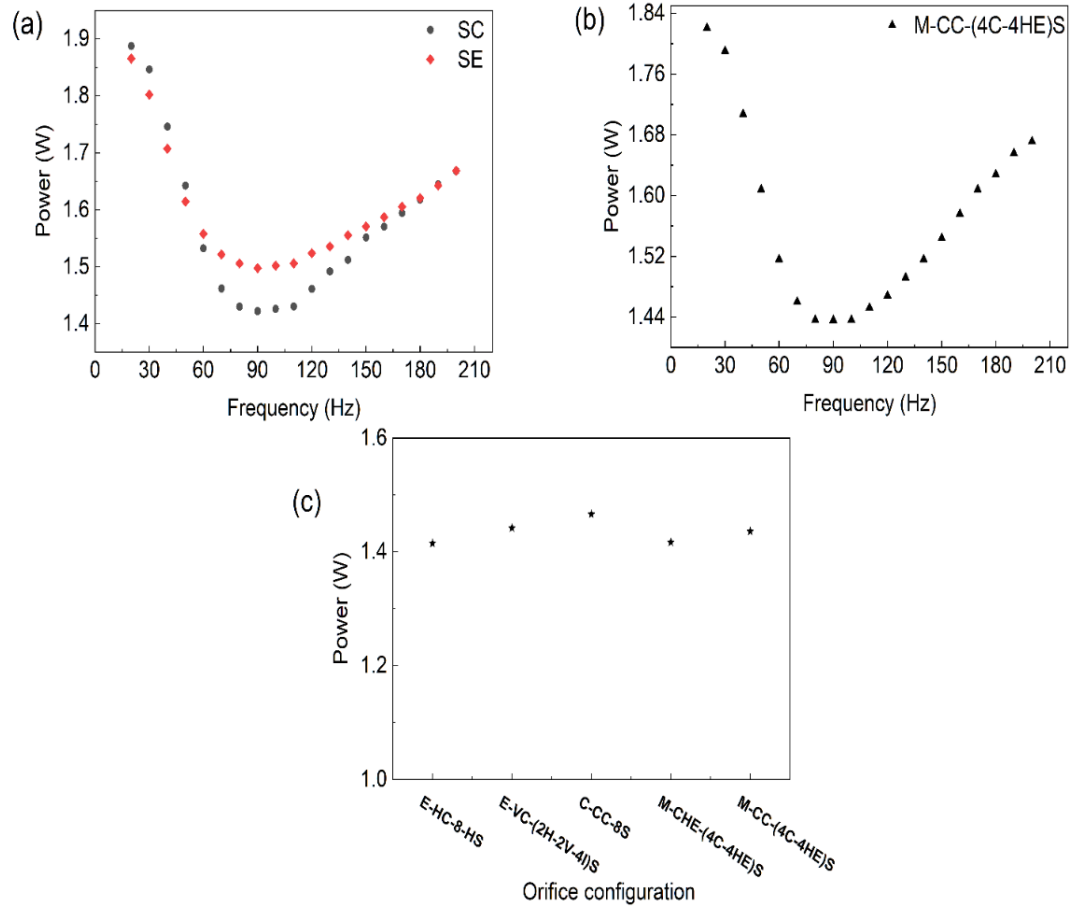


Fig. 4.3 power required as a function of frequency for (a) a single orifice (circular and elliptical) and (b) a multi-orifice configuration. (c) Power is required for various multi-orifice configurations at a resonance frequency (90 Hz).

In order to see the effect of z/d on centerline velocity for the multiple-orifices configurations is shown in Fig. 4.4. The maximum velocity is found at the orifice exit and decreases gradually. The SJ obtained from a single orifice is narrow compared with a multiple-orifice configuration. Therefore, the single orifice SJ covers a smaller portion of impingement of the heated surface as contrasted to the multiple-orifice configuration. A similar trend is also observed for other multiple-orifice configurations.

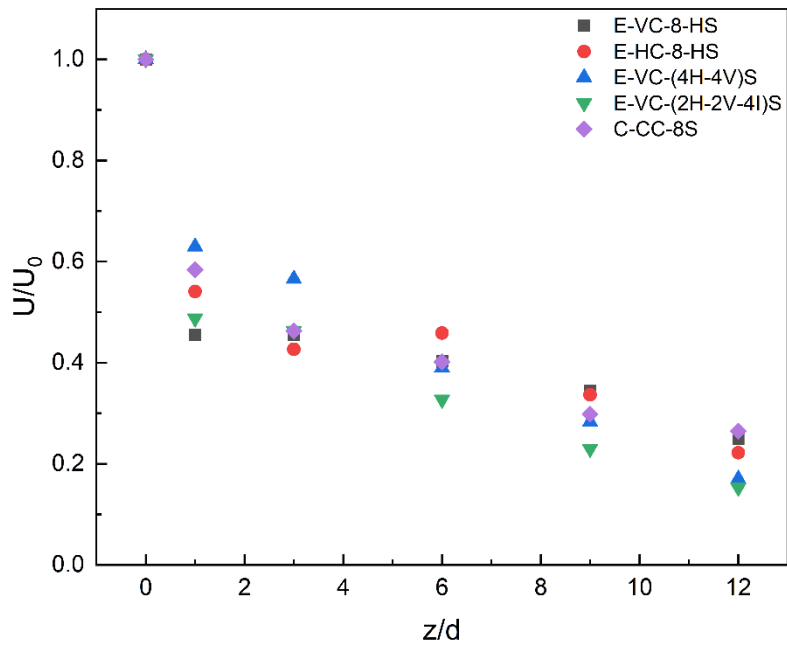


Fig. 4.4 Normalized centerline velocity as a function of z/d for different multiple-orifice configurations.

4.2. Heat transfer characteristics of single and multiple-orifice SJ

4.2.1. Comparison of single orifices (i.e., circular and elliptical)

This section discusses the heat transfer of SJ impingement from different single and multiple-orifice configurations. Table 1 provides the different types of configurations used for the study. The experiments are performed for SC ($D = 10$ mm) SE ($A.R.= 2$), multi- circular, multi- elliptical, and mixed (elliptical and circular) configurations. The SJA is operated at 90 Hz and maintains a constant amplitude of $4 V_{rms}$.

Fig. 4.5 shows the variation of the average Nusselt number (Nu_{avg}) with axial distance for the SC and SE orifices. It is observed that both orifices Nu_{avg} first increases (reach to upper limit) and then decrease with the boost in axial distance. This is because of alterations in the fluid flow qualities and Axis switching in jets issued from non-circular orifices, as explained by Miller et al.[84]. Additionally, the maximum Nu_{avg} is obtained for the elliptical orifice at a low axial distance. However, in the far-field, the Nu_{avg} for SE orifice is less than SC orifice.

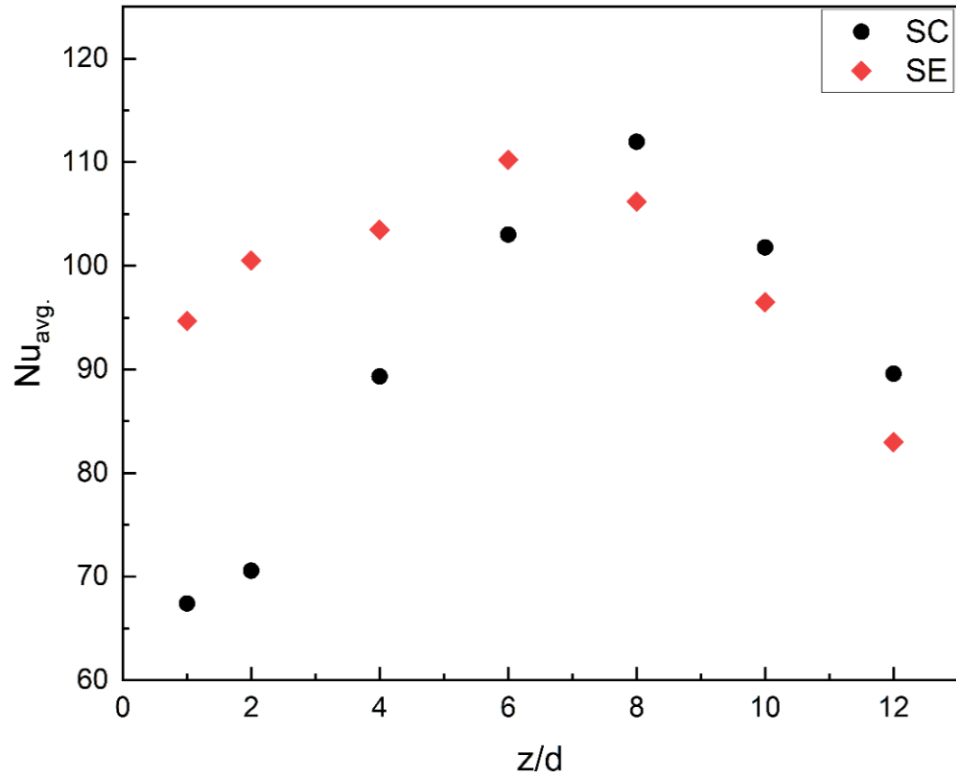


Fig. 4.5 Variation of Nu_{avg} for single circular and single elliptical orifice.

4.2.2. Comparison of multiple orifices

4.2.2.1. Comparison of single circular and multi- circular orifice SJ

The Nu_{avg} for single and multi-circular orifice configurations is presented in Fig. 4.6 . It shows that Nu_{avg} values obtained from the central orifice surrounded by satellite orifice (C-CC-8S) are exceeding as compared to those for SC orifice. In this direction, Mangate et al. [64] also found that SJ from the satellite orifice increases the entrainment of ambient fluid and gets combined with the jet from the center orifice, which has higher strength. It can be concluded that the C-CC-8S extracts a larger volume of heat from the warmed surface and the center orifice strongly manipulates the flow characteristics of the combined SJ at lower z/d .

4.2.2.2. Comparison of multi elliptical orifice SJ

The Fig. 4.7 demonstrates Nu_{avg} for different elliptical multi-orifice configurations at different z/d . Fig. 4.7 shows that configuration E-VC-(4H-4V)S was the best from the heat transfer perspective among all the studied elliptical multi-orifices. In this configuration, 4 elliptic satellite orifices have their axis perpendicular to the other 4 elliptic orifices.

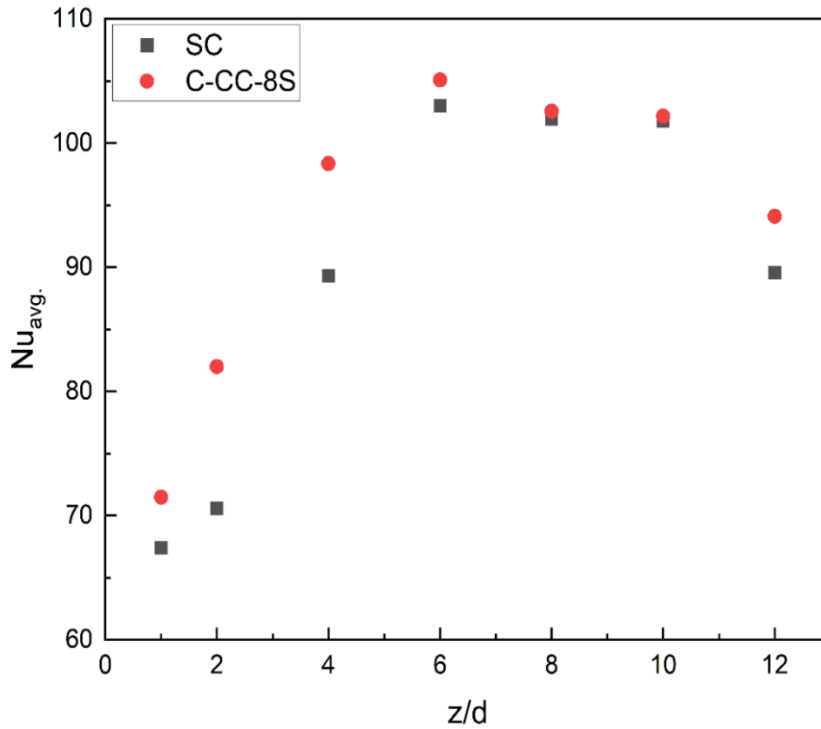


Fig. 4.6 Variation of Nu_{avg} for single and multi- circular orifice.

This arrangement causes enhanced mixing in the lower field as jets issued from both kinds of orifices exhibit axis switching. The perpendicularly oriented satellite orifices enable better fluid mixing and allow larger entrainment leading to an increase in the Nu_{avg} and heat transfer. Nu_{avg} for other configurations shows increasing nature up to $z/d = 6$ and then starts decreasing. However, E-VC-H-4V)S configuration Nu_{avg} increases up to $z/d = 8$. The jet issued from configuration E-HC-8HS is spreading lesser than that of configuration E-VC-(4H-4V)S. Therefore, configuration E-HC-8HS transfers more heat beyond $z/d = 8$ than configuration E-VC-(4H-4V)S. The SJ from other elliptical multi-orifice configurations is spreading more, allowing less surrounding low-temperature fluid to remove the heat from the high-temperature surface.

4.2.2.3. Selection from multi elliptical orifice configurations

In multi-orifice configurations, the jet issuing from satellite orifices gets indulged with fluid issuing from the central orifice and has more strength as the site of velocity and mass flux. Fig. 4.8 shows that multi-elliptical configurations outperform for most axial distances, i.e., multiple circular

orifice and baseline configurations (SC and SE orifice). Fig. 4.8 also reveals that a SE orifice has higher Nu_{avg} than multi-circular configuration C-CC-8S.

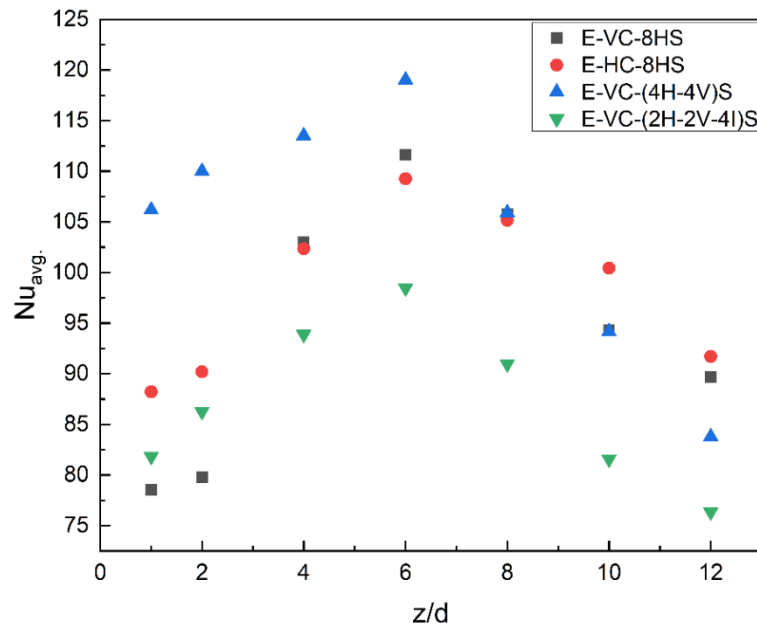


Fig. 4.7 Variation of Nu_{avg} for multi elliptical orifice configurations.

This signifies that the Axis switching phenomenon in a non-circular orifice significantly impacts heat transfer characteristics. The SE configuration is better than multi elliptical configurations (E-VC-(4H-4V)S and E-HC-8HS) for higher z/d . This is because jet issuing from multi orifice spreads more, allowing less entrainment and might imping beyond the heated surface in the far-field.

4.2.2.4. Mixed orifice configuration

Section 4.2.2.2 and 4.2.2.3 showed that the orientation of center and satellite orifices has a significant impact on the flow and heat transfer characteristics of SJ. In addition, it is already evident (Fig. 4.5) that elliptical orifice outperforms circular orifice at lower z/d and converse for the higher z/d . This phenomenon gave birth to the idea of using a combination of circular and elliptical orifices simultaneously for multi-orifice configuration. Fig. 4.9 illustrates the variation of Nu_{avg} with z/d . The Nu_{avg} first increases up to $z/d=6$ and then decreases. The M-CC-(4C-4HE)S shows the highest value of Nu_{avg} for almost every z/d . It has a circular orifice with a diameter of 5 mm at the center and has 4 circular and 4 elliptical orifices at the satellite position

alternately. It is found that the SJ issued from M-CC-(4C-4HE)S spreads less as compared to other mixed configurations. Thus, M-CC-(4C-4HE)S allows more surrounding air to interact with the heated plate and enables relatively higher heat transfer.

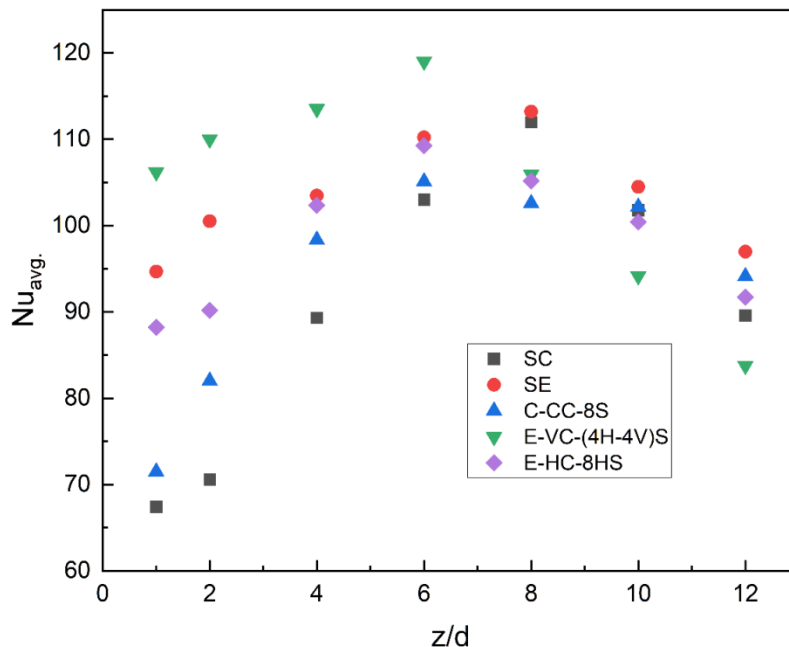


Fig. 4.8 Comparison of Nu_{avg} for two best multi elliptical orifices with multiple circular orifice (C-CC-8S) configurations along with baseline configurations (single circular (EC) and single elliptical (SE)).

4.2.2.5. Comparison of multi- elliptical and mixed configurations of orifice

Finally, Fig. 4.10 depicts the variation of Nu_{avg} for elliptical multi-orifice and mixed (combination of the circular and elliptical orifice) configuration. In section 4.2.2.3 it has already been discussed that among multi-elliptical configurations E-VC-(4H-4V)S performs better at low z/d and E-HC-8HS at high z/d . It is evident that at low z/d , E-VC-(4H-4V)S is the best among elliptical and mixed multi-orifice configurations, as shown in Fig. 4.10. However, at high z/d mixed configuration of orifice M-CC-(4C-4HE)S is the best. The mixed configuration allows the jet from different shapes of the orifice. Moreover, the elliptical satellite orifice exhibits axis switching mixed with the jet from the circular satellite orifice. Thus, the jet from the center circular orifice allows better mixing of the fluid and larger entrainment. The

more entrainment of surrounding fluid enhances the interaction of the fresh fluid with the hot surface and more heat transfer happens.

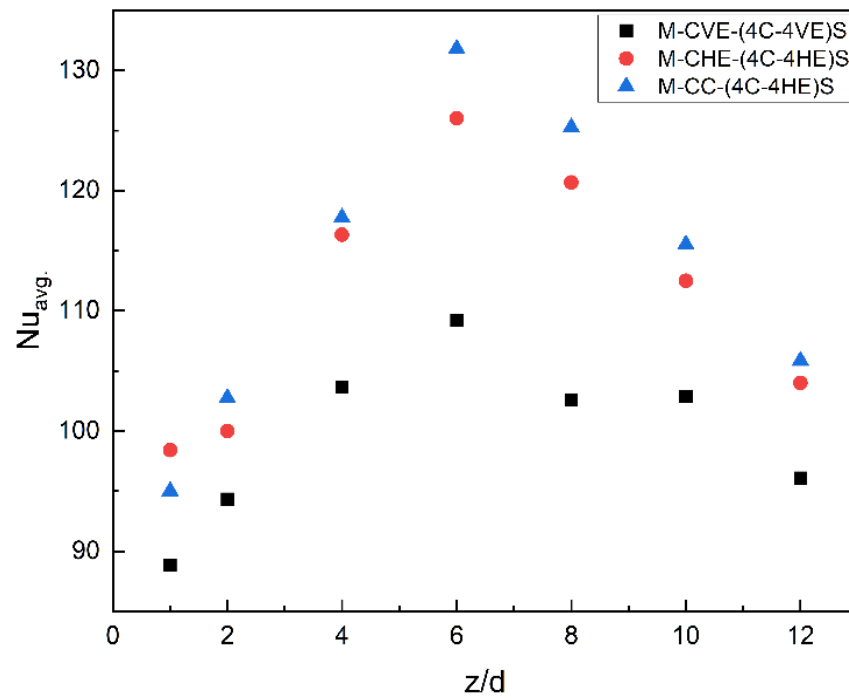


Fig. 4.9 Variation of Nu_{avg} as a function of Z/d for mixed configuration of orifices.

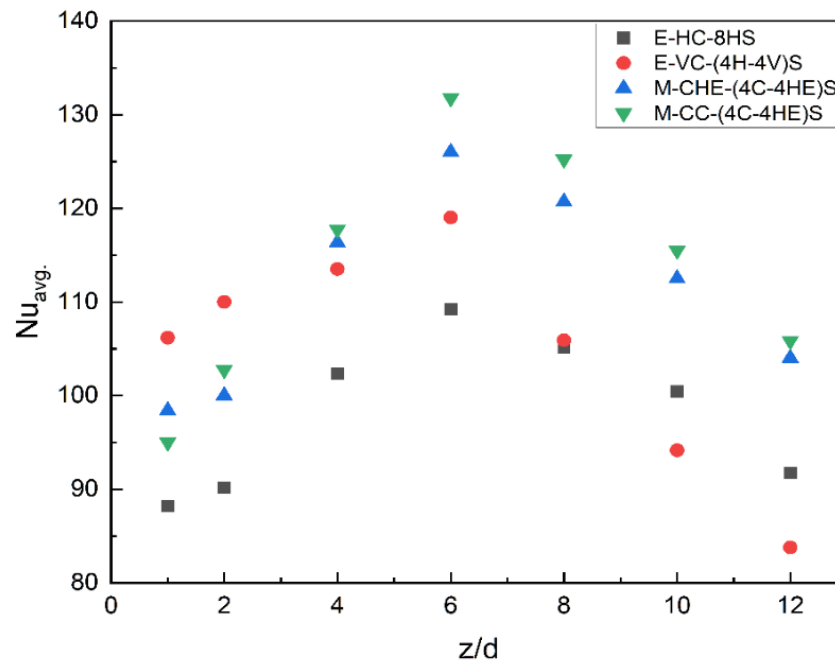


Fig. 4.10 Comparison of Nu_{avg} for multi-elliptical and mixed configuration.

Chapter 5

Synthetic Jet Impingement on a Vibrating Heated Surface

5.1. General background

There are several types of electrical gadgets and many of them have vibration-generating components. The vibrating parts substantially impact the life span of the device's auxiliary components, affecting the entire device's life. The vibration can be created by revolving pieces of a device, such as a rotating shaft in an electric motor, which creates a vibration of the device's essential components. When an axisymmetric jet impinges on a dynamic surface, the surface displacement can be classified into two directions: perpendicular to the jet axis and parallel to the jet axis. A surface moving horizontally, like a conveyor belt [85], and a surface rotating about the jet axis, likewise a rotor-stator system in a gas turbine [86]. Klein et al. [87] investigated heat transmission from a hot vibrating silicon chip put underneath a confined impinging micro-slot jet in the $756 < Re < 1260$ range. The silicon chip was oscillated at frequencies up to $f_s = 400$ Hz and micro amplitudes up to $a_s = 150$ μm using a piezoelectric actuator with a slot width of 220 μm . At the greatest displacement amplitude, the heat transfer coefficients are grown by 34% in the instance of $Re = 1260$, $f_s = 246$ Hz. They attributed the rise to the regeneration of the boundary layer driven by surface vibration-induced vortices. The influence of surface oscillation on local and average heat transfer coefficients was the focus of the preceding research instead of the impinging jet flow field. Although Ichimiya et al. [88] reported turbulence intensity data, the fluid dynamics of jet interaction with surface vibrations were not thoroughly investigated. Compared to a stationary surface, existing literature shows that surface oscillation increases and decreases jet impingement heat transfer. However, there are inadequate statistics to understand and establish the association between heat transfer and impinging-jet flow topographies owing to surface oscillation.

The jet impingement cooling of a vibrating surface is a relatively unexplored field of study. SJ impingement is an active cooling technology with high thermal efficiency making it an excellent choice for the thermal management of systems with vibrating parts.

5.2. Experimental setup

The experimental setup with a vibrating surface is shown in Fig. 5.1. The details of most of the experimental parts are explained in chapter 3. Here, the only difference is that a vibrating surface is used below the copper block. The assembly discussed above was made fastened with the vibration exciter (Syscon Instruments: SI-220) that was excited with the help of a power oscillator (Syscon Instruments: SI28-DR) and SJA was actuated by an addi-

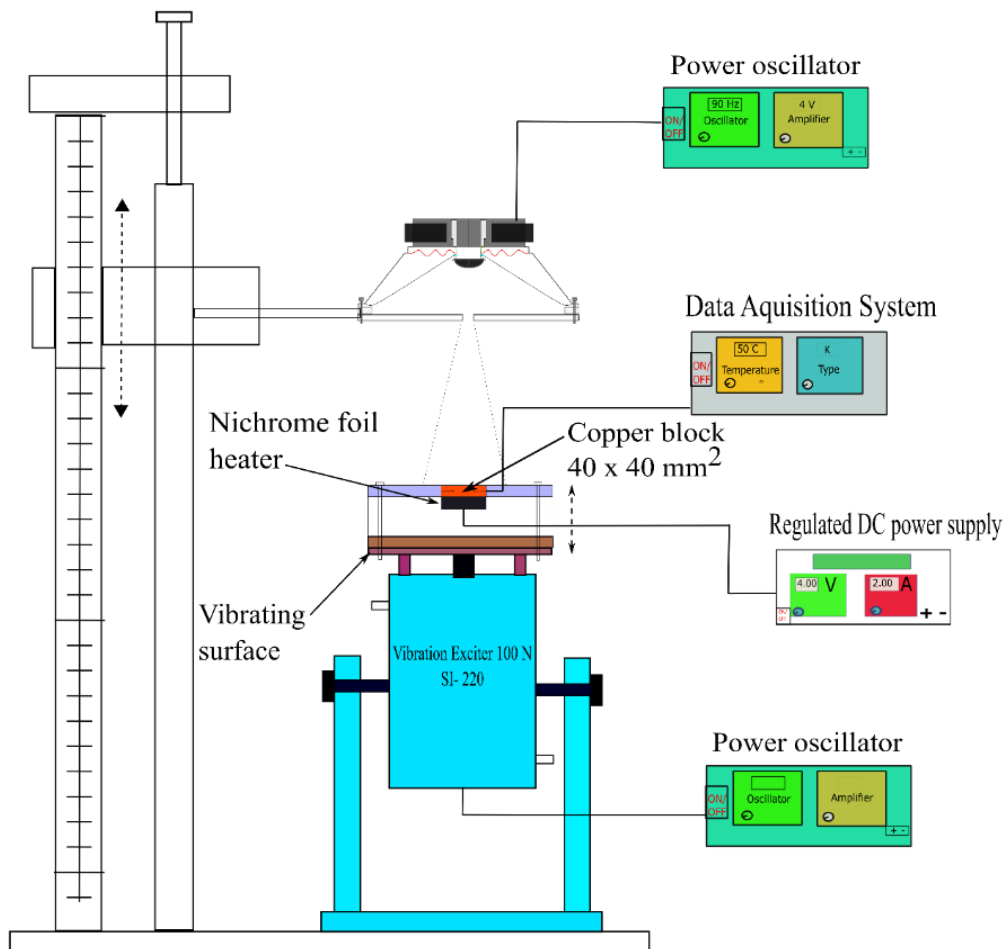


Fig. 5.1 Schematic of the setup for heat transfer from a vibrating surface.

-onal power oscillator of same specifications. The current supply and voltage drop across the copper block are determined using a digital multimeter (Fluke: 15B+). The SJ formation, measurement setup and conditions remained the same as those used in chapter 3.

5.3. Methodology

This section describes the experimental approach to investigate the effect of heated surface vibration frequency on synthetic jet impingement cooling for various z/d . First, an experiment was carried out to see if the amplitude of a vibration exciter remains constant while the frequency is changed. Given this objective, a laser diffraction sensor (LDS) was utilized, and the amplitude of the vibration exciter was found to be consistent over a frequency range of 5 Hz to 45 Hz for a stable power supply. At the same time, the speaker was actuated at the resonance frequency in order to obtain the optimum heat transfer. The heat was transferred from the vibrating surface using a single circular hole synthetic jet ($d= 10$ mm). A 2D-traversing stand adjusts the surface separation between the vibrating hot plate and orifice.

5.4. Results and discussion

Fig. 5.2 shows that heat transmission increases as the vibration frequency of the heated target surface increases. At an optimum value of z/d , heat transfer is maximal for all values of surface spacing (z/d) and frequencies of the heated surface.

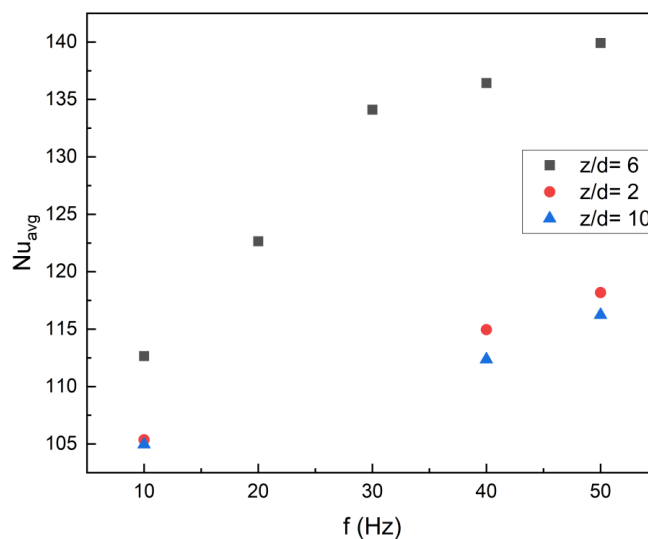


Fig. 5.2 Effect on Nu_{avg} due to vibration exciter frequency at different z/d .

This is because as the heated surface vibrates boundary layer produced over it will also vibrate, which allows heat to be transferred from the fluid inside the boundary layer to the fluid outside the boundary layer. This is because as the heated surface vibrates boundary layer produced over it will also vibrate, which allows heat to be transferred from the fluid inside the boundary layer to the fluid outside the boundary layer. As shown in Fig. 5.2, heat transfer was found to be low in the near field region due to jet confinement. However, heat transmission was found to be highest in the transitional zone due to boundary layer vibration, which would also have a threshold value. The heat transmission is minimal in the far-field zone because the jet velocity is low and spreading is greater.

Chapter- 6

Conclusions and the scope for future work

In this chapter, key inference obtained from the present work is highlighted. The scope for advanced research on multi-orifice synthetic jet impingement on heated vibrating surfaces is also discussed.

6.1. Conclusions

- The multi-orifice SJ exhibits better mixing compared to a single orifice.
- The time-averaged velocity measurements signify the interactions between the neighboring jets showed that synthetic jet from satellite orifices gets mixed with the jet issued from the center orifice at some axial distance.
- The mixed configuration of multi-orifice SJ demonstrates an interesting behavior of Nu_{avg} . The jet from the elliptical satellite orifice exhibits axis switching and simultaneously interacts with the jet from the circular satellite orifice and center orifice.
- In the case of lower z/d multi-elliptical orifice configuration E-VC-(4H-4V)S and higher z/d mixed configuration M-CC-(4C-4HE)S performs better heat transfer.
- A strong effect of shape and orientation of the satellite orifices on the heat transfer characteristics is observed and hence, significant from an application point of view.
- The heat transmission increases as the vibration frequency of the heated target surface increases. For an optimum value of z/d , heat transfer is maximal for all values of z/d at all frequencies.

6.2. Scope of future work

Synthetic jet impingement-based thermal managing system is widely used in abundant industrial purposes including electronic cooling. The present thesis reports the experimental study concerning the SJ-based systems incorporating multiple orifice jet-impingement and SJ on vibrating heated surfaces. SJs for heat transfer improvement are still in their early stages of development, with only a few studies published. Further, the heat transfer increase of heated flat plates is the focus of these studies. As a result, it is critical to explore the heat transfer properties of many test surface geometries exposed to SJ impingement to increase the heat transfer presentation of heat exchangers. From this study, some works that can be done in the future are suggested below:

- The curvature of concave/convex targets has a significant effect on jet recirculation and can be examined in the future.
- The flow and heat transfer performance of concave/convex target plates can be helpful for the thermal management of various electric devices.
- Thermal electric motor management can be done using synthetic jet impingement technique as it has vibrating elements.

References

- [1] C.S. Greco, G. Paolillo, A. Ianiro, G. Cardone and L. de Luca, *Effects of the stroke length and nozzle-to-plate distance on synthetic jet impingement heat transfer*, Int. J. Heat Mass Transf. 117 (2018), pp. 1019–1031.
- [2] M. Chaudhari, B. Puranik and A. Agrawal, *Multiple orifice synthetic jet for improvement in impingement heat transfer*, Int. J. Heat Mass Transf. 54 (2011), pp. 2056–2065.
- [3] A. Patapoutian, A.M. Peier, G.M. Story and V. Viswanath, *Thermotrp channels and beyond: Mechanisms of temperature sensation*, Nat. Rev. Neurosci. 4 (2003), pp. 529–539.
- [4] J.D. Greenspan, E.A. Roy, P.A. Caldwell and NS. Farooq, *Thermosensory intensity and affect throughout the perceptible range*, Somatosens. Mot. Res. 20 (2003), pp. 19–26.
- [5] G. Story, *The Emerging Role of TRP Channels in Mechanisms of Temperature and Pain Sensation*, Curr. Neuropharmacol. 4 (2006), pp. 183–196.
- [6] W.L. Cheng, N. Liu and W.F. Wu, *Studies on thermal properties and thermal control effectiveness of a new shape-stabilized phase change material with high thermal conductivity*, Appl. Therm. Eng. 36 (2012), pp. 345–352.
- [7] I. Sauciuc, R. Prasher, J.Y. Chang, H. Erturk, G. Chrysler, C.P. Chiu et al., *Thermal performance and key challenges for future CPU cooling technologies*, Proc. ASME Summer Heat Transf. Conf. 2 (2005), pp. 919–930.
- [8] R. Aschenbrenner, R.C. Pfahl and JM Bird, *The 2004 International Electronics Manufacturing Initiative (iNEMI) technology roadmaps*, 15th Eur. Microelectron. Packag. Conf. Exhib. EMPC 2005 - Conf. Program. Proc. (2005), pp. 401–405.
- [9] B. Agostini, M. Fabbri, J.E. Park, L. Wojtan, J.R. Thome and B. Michel, *State of the art of high heat flux cooling technologies*, Heat Transf. Eng. 28 (2007), pp. 258–281.
- [10] A. Pal, Y.K. Joshi, M.H. Beitelmal, C.D. Patel and T.M. Wenger, *Design and performance evaluation of a compact thermosyphon*, IEEE Trans. Components Packag. Technol. 25 (2002), pp. 601–607.
- [11] Y.F. Maydanik, S. V. Vershinin, M.A. Korukov and J.M. Ochterbeck, *Miniature loop heat pipes - A promising means for cooling electronics*, Thermomechanical Phenom. Electron. Syst. -Proceedings Intersoc. Conf. 2 (2004), pp. 60–66.

- [12] L. Jiang, J. Mikkelsen, J.M. Koo, D. Huber, S. Yao, L. Zhang et al., *Closed-loop electroosmotic microchannel cooling system for VLSI circuits*, IEEE Trans. Components Packag. Technol. 25 (2002), pp. 347–355.
- [13] X. Wei, *IMECE2004-62509*, (2016), pp. 1–7.
- [14] S. V. Garimella, V. Singhal and D. Liu, *On-chip thermal management with microchannel heat sinks and integrated micropumps*, Proc. IEEE 94 (2006), pp. 1534–1548.
- [15] J.S. Bintoro, A. Akbarzadeh and M. Mochizuki, *A closed-loop electronics cooling by implementing single phase impinging jet and mini channels heat exchanger*, Appl. Therm. Eng. 25 (2005), pp. 2740–2753.
- [16] R.E. Simons and R.C. Chu, *Application of thermoelectric cooling to electronic equipment: A review and analysis*, Annu. IEEE Semicond. Therm. Meas. Manag. Symp. (2000), pp. 1–9.
- [17] Y.J. Kim, Y.K. Joshi and A.G. Fedorov, *An absorption based miniature heat pump system for electronics cooling*, Int. J. Refrig. 31 (2008), pp. 23–33.
- [18] N. Ivanova, V. Gugleva, M. Dobрева, I. Pehlivanov, S. Stefanov and V. Andonova, *We are IntechOpen , the world ' s leading publisher of Open Access books Built by scientists , for scientists TOP 1 %*, Intech i (2016), pp. 13.
- [19] R. Mahalingam and A. Glezer, *Air cooled heat sinks integrated with synthetic jets*, Intersoc. Conf. Therm. Thermomechanical Phenom. Electron. Syst. IThERM 2002-Janua (2002), pp. 285–291.
- [20] J. Zhou, H. Tang and S. Zhong, *Vortex roll-up criterion for synthetic jets*, AIAA J. 47 (2009), pp. 1252–1262.
- [21] B.L. Smith and A. Glezer, *The formation and evolution of synthetic jets*, Phys. Fluids 10 (1998), pp. 2281–2297.
- [22] S.G. Mallinson, G. Hong and J.A. Reizes, *Some characteristics of synthetic jets*, 30th Fluid Dyn. Conf. (1999), .
- [23] S.G. Mallinson, C.Y. Kwok and J.A. Reizes, *Numerical simulation of micro-fabricated zero mass-flux jet actuators*, Sensors Actuators, A Phys. 105 (2003), pp. 229–236.
- [24] S. Mallinson and J. Reizes, *Numerical Simulation of Membrane Forcing Effects On Synthetic Jet Actuator Flows*, 14th Australas. FluidMechanics Conf. (2001), pp. 757–760.
- [25] J.R. Guarino and V.P. Manno, *Characterization of laminar jet impingement cooling in portable computer applications*, Annu. IEEE

Semicond. Therm. Meas. Manag. Symp. 25 (2001), pp. 337–346.

[26] T. Mahmud, J.N. Haque, K.J. Roberts, D. Rhodes and D. Wilkinson, *Measurements and modelling of free-surface turbulent flows induced by a magnetic stirrer in an unbaffled stirred tank reactor*, Chem. Eng. Sci. 64 (2009), pp. 4197–4209.

[27] L. Le Van, C. Nguyen Nhu, T.N. Tai, T. Xuan Dinh, C.D. Tran, L.D. Bao et al., *Liquid Pumping and Mixing by Pzt Synthetic Jet*, 2019 20th Int. Conf. Solid-State Sensors, Actuators Microsystems Eurosensors XXXIII, TRANSDUCERS 2019 EUROSensors XXXIII (2019), pp. 198–201.

[28] M. Al-Atabi, *Experimental investigation of the use of synthetic jets for mixing in vessels*, J. Fluids Eng. Trans. ASME 133 (2011), pp. 2011–2014.

[29] M. Arik, Y. Utturkar and M. Ozmusul, *Effect of synthetic jets over natural convection heat sinks*, ASME Int. Mech. Eng. Congr. Expo. Proc. 10 (2009), pp. 511–517.

[30] C. SINGH, D. Manani, K. Mathiyazhagan, P. Sharma and F. Hakkak, *Department of Mechanical Engineering*, Technology 169 (2010), pp. 178.

[31] B.L. Smith and A. Glezer, *Jet vectoring using synthetic jets*, J. Fluid Mech. 458 (2002), pp. 1–34.

[32] N. Ramos-Pedroza, W. MacKunis and M. Reyhanoglu, *Synthetic Jet Actuator-Based Aircraft Tracking Using a Continuous Robust Nonlinear Control Strategy*, Int. J. Aerosp. Eng. 2017 (2017), .

[33] G. Zhao, Q. Zhao, Y. Gu and X. Chen, *Experimental investigations for parametric effects of dual synthetic jets on delaying stall of a thick airfoil*, Chinese J. Aeronaut. 29 (2016), pp. 346–357.

[34] TT Rice, K. Taylor and M. Amitay, *Pulse modulation of synthetic jet actuators for control of separation*, Phys. Rev. Fluids 6 (2021), pp. 1–28.

[35] J.W. Wiltse, *United States Patent (19) SYNTHETICJET ACTUATORS FOR MIXING*, (2000), .

[36] M. Krieg and K. Mohseni, *Thrust characterization of a bioinspired vortex ring thruster for locomotion of underwater robots*, IEEE J. Ocean. Eng. 33 (2008), pp. 123–132.

[37] M. Chaudhari, B. Puranik and A. Agrawal, *Heat transfer characteristics of synthetic jet impingement cooling*, Int. J. Heat Mass Transf. 53 (2010), pp. 1057–1069.

[38] M.B. Gillespie, W.Z. Black, C. Rinehart and A. Glezer, *Local convective heat transfer from a constant heat flux flat plate cooled by synthetic air jets*, J. Heat Transfer 128 (2006), pp. 990–1000.

- [39] A. Pavlova and M. Amitay, *Electronic cooling using synthetic jet impingement*, J. Heat Transfer 128 (2006), pp. 897–907.
- [40] O. Ghaffari, S.A. Solovitz and M. Arik, *An investigation into flow and heat transfer for a slot impinging synthetic jet*, Int. J. Heat Mass Transf. 100 (2016), pp. 634–645.
- [41] C.Y.Y. Lee, M.L. Woyciekoski and J.B. Copetti, *Experimental study of synthetic jets with rectangular orifice for electronic cooling*, Exp. Therm. Fluid Sci. 78 (2016), pp. 242–248.
- [42] E. Fanning, T. Persoons and D.B. Murray, *Heat transfer characteristics of a pair of impinging synthetic jets: Effect of orifice spacing and impingement distance*, J. Phys. Conf. Ser. 395 (2012), .
- [43] O. Ghaffari, M. Ikhlaq and M. Arik, *An experimental study of impinging synthetic jets for heat transfer augmentation*, Int. J. Air-Conditioning Refrig. 23 (2015), pp. 1–11.
- [44] C.S. Greco, A. Ianiro and G. Cardone, *Time and phase average heat transfer in single and twin circular synthetic impinging air jets*, Int. J. Heat Mass Transf. 73 (2014), pp. 776–788.
- [45] L. Silva-Llanca, A. Ortega and I. Rose, *Experimental convective heat transfer in a geometrically large two-dimensional impinging synthetic jet*, Int. J. Therm. Sci. 90 (2015), pp. 339–350.
- [46] L. Silva-Llanca, *Replicating impinging synthetic jets as a train of consecutive viscous Lamb-Ossen vortex pairs*, Proc. 15th Intersoc. Conf. Therm. Thermomechanical Phenom. Electron. Syst. ITherm 2016 (2016), pp. 930–938.
- [47] L. Silva-Llanca and A. Ortega, *Vortex dynamics and mechanisms of heat transfer enhancement in synthetic jet impingement*, Int. J. Therm. Sci. 112 (2017), pp. 153–164.
- [48] P. Valiorgue, T. Persoons, A. McGuinn and D.B. Murray, *Heat transfer mechanisms in an impinging synthetic jet for a small jet-to-surface spacing*, Exp. Therm. Fluid Sci. 33 (2009), pp. 597–603.
- [49] M. Hatami, F. Bazdidi-Tehrani, A. Abouata and A. Mohammadi-Ahmar, *Investigation of geometry and dimensionless parameters effects on the flow field and heat transfer of impingement synthetic jets*, Int. J. Therm. Sci. 127 (2018), pp. 41–52.
- [50] A. Jacob, S.K. A and K.E.R. Roy, *Effects of Frequency and Jet to Surface Spacing on Synthetic Jet Impingement Heat Transfer*, Int. J. Eng. Adv. Technol. 9 (2020), pp. 665–660.
- [51] B. Giachetti, M. Fénot, D. Couton and F. Plourde, *Influence of*

Reynolds number synthetic jet dynamic in crossflow configuration on heat transfer enhancement, Int. J. Heat Mass Transf. 118 (2018), pp. 1–13.

[52] A. McGuinn, R. Farrelly, T. Persoons and D.B. Murray, *Flow regime characterisation of an impinging axisymmetric synthetic jet*, Exp. Therm. Fluid Sci. 47 (2013), pp. 241–251.

[53] C.S. Greco, G. Cardone and J. Soria, *On the behaviour of impinging zero-net-mass-flux jets*, J. Fluid Mech. 810 (2017), pp. 25–59.

[54] D.I. Rylatt and T.S. O’Donovan, *The effects of stroke length and Reynolds number on heat transfer to a ducted confined and semi-confined synthetic air jet*, J. Phys. Conf. Ser. 525 (2014), .

[55] C.S. Greco, A. Ianiro, T. Astarita and G. Cardone, *On the near field of single and twin circular synthetic air jets*, Int. J. Heat Fluid Flow 44 (2013), pp. 41–52.

[56] P.K. Singh, S.K. Sahu, P.K. Upadhyay and A.K. Jain, *Experimental investigation on thermal characteristics of hot surface by synthetic jet impingement*, Appl. Therm. Eng. 165 (2020), pp. 114596.

[57] U.S. Bhapkar, A. Srivastava and A. Agrawal, *Acoustic and heat transfer characteristics of an impinging elliptical synthetic jet generated by acoustic actuator*, Int. J. Heat Mass Transf. 79 (2014), pp. 12–23.

[58] M. Chaudhari, B. Puranik and A. Agrawal, *Effect of orifice shape in synthetic jet based impingement cooling*, Exp. Therm. Fluid Sci. 34 (2010), pp. 246–256.

[59] M. Jain, B. Puranik and A. Agrawal, *A numerical investigation of effects of cavity and orifice parameters on the characteristics of a synthetic jet flow*, Sensors Actuators, A Phys. 165 (2011), pp. 351–366.

[60] S. Zhong, L. Garcillan, Z. Pokusevski and NJ Wood, *A PIV study of synthetic jets with different orifice shape and orientation*, in 2nd AIAA Flow Control Conference, 2004.

[61] L. Oren, E. Gutmark, S. Muragappan and S. Khosla, *Flow characteristics of non circular synthetic jets*, 47th AIAA Aerosp. Sci. Meet. Incl. New Horizons Forum Aerosp. Expo. (2009), .

[62] M.H. Hong, S.Y. Cheng and S. Zhong, *Effect of geometric parameters on synthetic jet: A review*, Phys. Fluids 32 (2020), .

[63] P.K. Singh, S.K. Sahu, P.K. Upadhyay and A.K. Jain, *Experimental investigation on thermal characteristics of hot surface by synthetic jet impingement*, Appl. Therm. Eng. 165 (2020), pp. 114596.

[64] L. Mangate, H. Yadav, A. Agrawal and M. Chaudhari, *Experimental*

investigation on thermal and flow characteristics of synthetic jet with multiple-orifice of different shapes, Int. J. Therm. Sci. 140 (2019), pp. 344–357.

[65] T. Persoons, T.S. O’Donovan and D.B. Murray, *Heat transfer in adjacent interacting impinging synthetic jets*, Proc. ASME Summer Heat Transf. Conf. 2009, HT2009 1 (2009), pp. 955–962.

[66] A. Arshad, M. Jabbal and Y. Yan, *Synthetic jet actuators for heat transfer enhancement – A critical review*, Int. J. Heat Mass Transf. 146 (2020), pp. 118815.

[67] A. Crook, W.J. Crowther and NJ Wood, *A PARAMETRIC STUDY OF A SYNTHETIC JET IN A CROSS FLOW*, .

[68] LD. Mangate and M.B. Chaudhari, *Heat transfer and acoustic study of impinging synthetic jet using diamond and oval shape orifice*, Int. J. Therm. Sci. 89 (2015), pp. 100–109.

[69] KBMQ. Zaman, *Axis switching and spreading of an asymmetric jet - Role of vorticity dynamics*, 33rd Aerosp. Sci. Meet. Exhib. 316 (1995), pp. 1–27.

[70] P.J. Lu, *Streamwise Evolution of a Square Jet Cross Section*, AIAA J. 30 (1992), pp. 2852–2857.

[71] F. Hussain and H.S. Husain, *Journal of Fluid Mechanics Digital Archive Volume 208 issue 1989 [doi 10.1017%2FS0022112089002843] Fazle Hussain and Hyder S. Husain -- Elliptic jets. Part 1. Charact*, 208 (1989), .

[72] M. Chaudhari, G. Verma, B. Puranik and A. Agrawal, *Frequency response of a synthetic jet cavity*, Exp. Therm. Fluid Sci. 33 (2009), pp. 439–448.

[73] B.L. Smith and A. Glezer, *Vectoring of adjacent synthetic jets*, AIAA J. 43 (2005), pp. 2117–2124.

[74] X. Deng, Z. Luo, Z. Xia, W. Gong and L. Wang, *Active-passive combined and closed-loop control for the thermal management of high-power LED based on a dual synthetic jet actuator*, Energy Convers. Manag. 132 (2017), pp. 207–212.

[75] Z.B. Luo, X. Deng, Z.X. Xia, L. Wang and W.J. Gong, *Flow field and heat transfer characteristics of impingement based on a vectoring dual synthetic jet actuator*, Int. J. Heat Mass Transf. 102 (2016), pp. 18–25.

[76] D.E. Metzger, T. Yamashita and C.W. Jenkins, *Impingement cooling of concave surfaces with lines of circular air jets*, J. Eng. Gas Turbines Power 91 (1969), pp. 149–155.

[77] D.H. Lee, Y.S. Chung and SY Won, *The effect of concave surface*

curvature on heat transfer from a fully developed round impinging jet, Int. J. Heat Mass Transf. 42 (1999), pp. 2489–2497.

[78] M. Fenot, E. Dorignac and J.J. Vullierme, *An experimental study on hot round jets impinging a concave surface*, Int. J. Heat Fluid Flow 29 (2008), pp. 945–956.

[79] C. Gau and C.M. Chung, *Surface curvature effect on slot- air-jet impingement cooling flow and heat transfer process*, J. Heat Transfer 113 (1991), pp. 858–864.

[80] Y. LYU, J. ZHANG, X. LIU and Y. SHAN, *Experimental study of single-row chevron-jet impingement heat transfer on concave surfaces with different curvatures*, Chinese J. Aeronaut. 32 (2019), pp. 2275–2285.

[81] R. Holman, Y. Utturkar, R. Mittal, B.L. Smith and L. Cattafesta, *Formation criterion for synthetic jets*, AIAA J. 43 (2005), pp. 2110–2116.

[82] R. Mahalingam and A. Glezer, *Design and thermal characteristics of a synthetic jet ejector heat sink*, J. Electron. Packag. Trans. ASME 127 (2005), pp. 172–177.

[83] K. Yogi, M.M. Godase, M. Shetty, S. Krishnan and S. V. Prabhu, *Experimental investigation on the local heat transfer with a circular jet impinging on a metal foamed flat plate*, Int. J. Heat Mass Transf. 162 (2020), pp. 120405.

[84] P. Grvrt, *NUMERICAL SIMULATION OF NON-CIRCULAR JETS*, 24 (1995), .

[85] J. Senter and C. Sollicec, *Flow field analysis of a turbulent slot air jet impinging on a moving flat surface*, Int. J. Heat Fluid Flow 28 (2007), pp. 708–719.

[86] TD. Nguyen, J. Pellé, S. Harmand and S. Poncet, *PIV measurements of an air jet impinging on an open rotor-stator system*, Exp. Fluids 53 (2012), pp. 401–412.

[87] D. Klein and G. Hetsroni, *Enhancement of heat transfer coefficients by actuation against an impinging jet*, Int. J. Heat Mass Transf. 55 (2012), pp. 4183–4194.

[88] K. Ichimiya and Y. Yoshida, *Oscillation effect of impingement surface on two-dimensional impingement heat transfer*, J. Heat Transfer 131 (2009), pp. 1–6.